NASA Contractor Report 3139

A Study of Scattering, Production, and Stimulated Emission of Sound by Vortex Flows

John E. Yates

CONTRACT NAS1-15033
MAY 1979

NASA

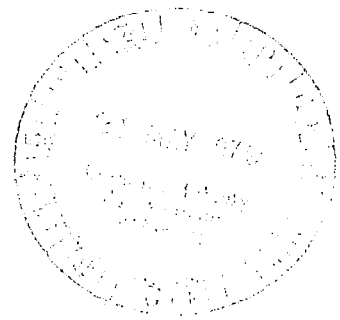

NASA Contractor Report 3139

A Study of Scattering, Production, and Stimulated Emission of Sound by Vortex Flows

John E. Yates
Aeronautical Research Associates of Princeton, Inc.
Princeton, New Jersey

Prepared for
Langley Research Center
under Contract NAS1-15033

National Aeronautics
and Space Administration

Scientific and Technical Information Office

1979

TABLE OF CONTENTS

SUMMARY

The basic theory of aeroacoustics of homentropic fluid media presented in Reference 1 is applied to the problems of sound scattering, production, and stimulated emission. A general theory of scattering from low speed three-dimensional vortex flows is presented. Specific results are given for the horseshoe vortex and vortex ring. The noise of an elementary corotating vortex pair in various flows is calculated. It is shown that a potential flow and shear flow can substantially increase the basic pair noise. Small reverse shears can annihilate vortex pairs and eliminate the pair noise mechanism. The pair results are used to explain qualitatively the operation of noise suppression devices. The stimulated emission of a single vortex pair and four and six vortex arrays is demonstrated. The results for six vortices illustrate how external pure tones can amplify the broadband noise of a jet in agreement with recent experimental evidence.

I. INTRODUCTION

The present report is a supplement to NASA CR 2987 (Ref. 1) and the reader is referred to the original report for a detailed discussion of the underlying concepts, theory, and initial application to the three basic problems of aeroacoustics. In Section II of this report the scattering of sound from three-dimensional low Mach number vortex flows is considered. Specific examples include the horseshoe vortex and vortex ring. The remainder of the report describes a collection of numerical experiments that illustrate how the noise of elementary vortex flows (in particular, the corotating pair) can be enhanced or altered by various mean flows and sound. The noise of a vortex pair in a shear flow is given particular attention. The final numerical examples illustrate the problem of vortex flow stimulation by an externally applied sound field. For a small collection of vortices, it is shown that a discrete tone can amplify the broadband noise in agreement with experimental results (Refs. 2 and 3).

NOMENCLATURE

a_∞	isentropic sound speed
db	decibel
$\vec{D}(\vec{y})$ or $D^i(\vec{y})$	see Eqs. (3.4) and (3.12)
$\mathcal{H}$	Bernoulli enthalpy, see Eq. (2.2)
$H(x)$	Heaviside step function
i	$\sqrt{-1}$
$J_n(z)$	Bessel function
$\vec{k}$	wave vector
$\vec{L}$	Coriolis acceleration, see Eq. (3.18)
L,D	see Figures 4.2 and 4.9
M	Mach number
OASPL	overall sound pressure level
p	pressure
p_{ref}	2×10^{-5} newtons/(meter)^2
$Q_{ij}(\vec{y})$	see Eqs. (3.8) and (3.13)
R	$\lvert\vec{y}\rvert$
$R(\tau)$	pressure autocorrelation, see Eq. (3.24)
$S(\omega)$	spectrum, see Eq. (3.22)
$S_c(\theta)$	scattering function, see Eq. (3.24)
t	time
T	period of rotation of a vortex pair in a shear flow, see Eq. (3.30) and Figure 3.3
T_c, T_m	see Eqs. (2.12) and (2.13)
$T^{ijk}(\vec{y})$	see Eqs. (3.8) and (3.14)
$\vec{u}_o$	steady flow velocity, see Eq. (2.4)

$U(y)$	two-dimensional shear flow, see Figure 3.2
$\vec{V}(\vec{x},t)$	external velocity field, see Figure 3.1
$\overset{\circ}{V}_n^i, \overset{\circ\circ}{V}_n^i$	see Eq. (3.10)
$\vec{x}_n$	vector position of a vortex, see Figure 3.1
$\vec{x}_{nm}$	see Eq. (3.3)
$\vec{x}, \vec{y}$	position vectors
γ_n	$\Gamma_n/2\pi$, see Figure 3.1
Γ	circulation of a vorticity distribution
Γ_n	total strength (circulation) of a two-dimensional vortex
δ	see Eq. (3.31)
δ_{ij}	see Eq. (3.9)
$\delta(z)$	delta function
ε_{ij}	see Eq. (3.9)
λ	see Eq. (3.31)
ρ_∞	density of ambient medium
ϕ	velocity potential
ω	radian frequency
$\vec{\omega}_o$	curl $\vec{u}_o$, vorticity
Ω	two-dimensional vorticity distribution

SPECIAL NOTATION

$\frac{D}{Dt}$	convective operator, see Eq. 2.3
div, grad, curl, ∇^2	usual vector operations
$(\vec{\ })$	denotes vector quantity
$(\hat{\ })$	denotes unit vector

$\|\ \|$	absolute value of vector quantity
$(\cdot)$	denotes dot product
(x)	denotes cross product
$(*)$	denotes three-dimensional spatial Fourier transform

II. THREE-DIMENSIONAL SCATTERING THEORY

Consider the problem of sound scattering from a weak flowfield. The appropriate equations are (Ref. 1, p. 24)

$$\frac{1}{a_\infty^2}\frac{D^2\phi}{Dt^2} - \nabla^2\phi = \frac{1}{a_\infty^2}\frac{\partial \mathcal{H}}{\partial t} \tag{2.1}$$

$$\nabla^2\mathcal{H} = \text{div}(\text{grad}\,\phi \times \vec{\omega}_o) \tag{2.2}$$

where

$$\frac{D}{Dt} = \frac{\partial}{\partial t} + \vec{u}_o \cdot \text{grad} \tag{2.3}$$

and $\vec{u}_o$, $\vec{\omega}_o$ are the velocity and vorticity fields of a quasi-steady incompressible flow; i.e.,

$$\vec{u}_o = \text{curl}\,\frac{1}{4\pi}\int \frac{\vec{\omega}_o(\vec{y})}{|\vec{x} - \vec{y}|}\,d\vec{y} \tag{2.4}$$

The acoustic pressure is given by

$$\begin{aligned} p &= -\rho_\infty\left(\frac{D\phi}{Dt} - \mathcal{H}\right) \\ &\sim -\rho_\infty\frac{\partial\phi}{\partial t} \quad \text{farfield} \end{aligned} \tag{2.5}$$

Assume an incident plane wave and calculate the scattered field; i.e.,

$$p = \left(p_i e^{i\vec{k}\cdot\vec{x}} + p_s \right) e^{-i\omega t} \tag{2.6}$$

with

$$k\, a_\infty = \omega \tag{2.7}$$

To lowest order (Born approximation) the scattered sound field satisfies the following equations:

$$\nabla^2 p_s + k^2 p_s = -\rho_\infty k^2 (\mathcal{H} - 2\vec{u}_o \cdot \text{grad}\ \phi_i) \tag{2.8}$$

$$\nabla^2 \mathcal{H} = \text{div}(\text{grad}\ \phi_i \times \vec{\omega}_o) \tag{2.9}$$

$$\phi_i = p_i / i\omega\rho_\infty \tag{2.10}$$

The scattered farfield is given by

$$p_s = \frac{\rho_\infty k^2 e^{ik|\vec{x}|}}{4\pi|\vec{x}|} (T_c + T_m) \tag{2.11}$$

with

$$T_c = \int e^{-ik\hat{x}\cdot\vec{y}}\, \mathcal{H}\, d\vec{y} \tag{2.12}$$

$$T_m = -2 \int e^{-ik\hat{x}\cdot\vec{y}}\, \vec{u}_o \cdot \text{grad}\ \phi_i\, d\vec{y} \tag{2.13}$$

The two parts of the scattered field result from the vortex core and potential flow mantle of the given incompressible flow.

Because of the Biot-Savart relation (2.4), both the core and mantle scattering can be conveniently expressed in terms of the core vorticity. First, take the Fourier transform of (2.9) to obtain

$$T_c = - \frac{ip_i}{\rho_\infty a_\infty k^2} (\hat{x}x\vec{k}) \cdot \int e^{-i(k\hat{x}-\vec{k})\cdot\vec{y}} \vec{\omega}_o \, d\vec{y} \tag{2.14}$$

where (2.6) and (2.10) have been used. The mantle scattering can similarly be expressed in terms of $\vec{\omega}_o$; thus,

$$T_m = - \frac{2p_i}{\rho_\infty a_\infty} \frac{\vec{k}}{k} \cdot \int e^{-i(k\hat{x}-\vec{k})\cdot\vec{y}} \vec{u}_o \, d\vec{y} \tag{2.15}$$

$$= \frac{2ip_i}{\rho_\infty a_\infty} \frac{(\hat{x}x\vec{k})}{|k\hat{x} - \vec{k}|^2} \cdot \int e^{-i(k\hat{x}-\vec{k})\cdot\vec{y}} \vec{\omega}_o \, d\vec{y}$$

where the Biot-Savart relation (2.4) has been used. The combined core and mantle scattered sound field is

$$p_s = \frac{ikp_i e^{ik|\vec{x}|}}{2\pi a_\infty |\vec{x}|} \frac{(\hat{x}\cdot\vec{k})(\hat{x}x\vec{k})}{|k\hat{x} - \vec{k}|^2} \cdot \vec{\omega}_o^*(k\hat{x} - \vec{k}) \tag{2.16}$$

where

$$\vec{\omega}_o^*(\vec{\lambda}) = \int e^{-i\vec{\lambda}\cdot\vec{y}} \vec{\omega}_o(\vec{y}) \, d\vec{y} \tag{2.17}$$

is the three-dimensional Fourier transform of the vorticity field. The last result is particularly convenient for calculating the scattered sound field. Several important examples are discussed below.

1) Vortex Core

The first example is the three-dimensional analogy of the scattering from a vortex core (see Ref. 1, p. 24).

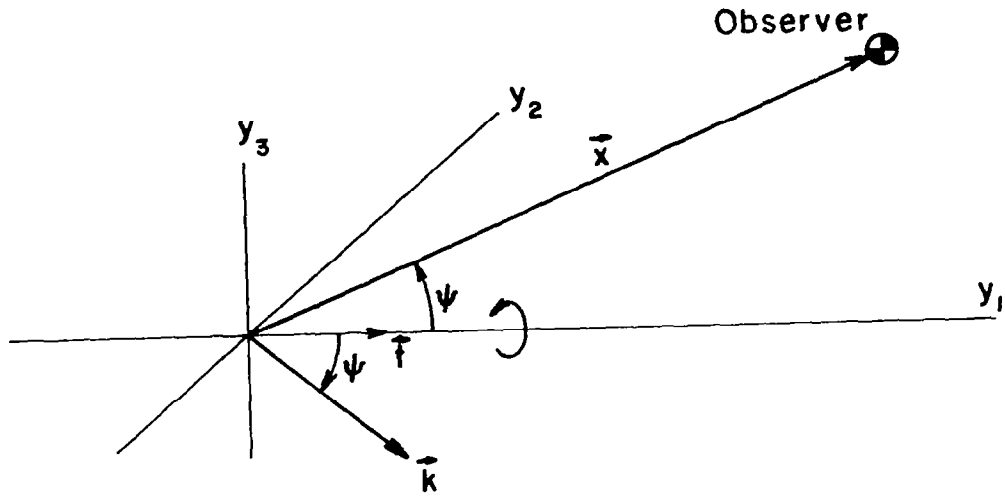

$$\vec{\omega}_o = \vec{t}\Omega\left(\vec{y}_\perp\right)$$

$$\vec{y}_\perp = \vec{y} - \left(\vec{t}\cdot\vec{y}\right)\vec{t} \qquad (2.18)$$

$$\vec{\lambda}_\perp = \vec{\lambda} - \left(\vec{t}\cdot\vec{\lambda}\right)\vec{t}$$

and

$$\vec{\omega}_o^*\left(\vec{\lambda}\right) = \vec{t}\int_{-\infty}^{\infty} e^{-i\lambda_{||}z_{||}}\, dz_{||} \int e^{-i\vec{\lambda}_\perp\cdot\vec{y}_\perp}\, \Omega\left(\vec{y}_\perp\right) d\vec{y}_\perp \qquad (2.19)$$

$$= 2\pi\vec{t}\ \delta\left(\vec{\lambda}\cdot\vec{t}\right)\int e^{-i\vec{\lambda}_\perp\cdot\vec{y}_\perp}\, \Omega\left(\vec{y}_\perp\right) d\vec{y}_\perp$$

The delta function in (2.19) implies that all of the scattered sound is emitted in the cone defined by

$$\hat{x} \cdot \vec{t} = \frac{\vec{k}}{k} \cdot \vec{t} \tag{2.20}$$

If the incident plane wave makes an angle ψ with the vortex axis as shown in the sketch, then all of the scattered sound is emitted in the cone with semi-vertex angle ψ. For an axisymmetric core with $\vec{k}$ normal to the core axis, (2.19) reduces to

$$\vec{\omega}_o^* = 2\pi \Gamma \vec{t} \, \delta\left(\vec{\lambda} \cdot \vec{t}\right) S_c(\theta) \tag{2.21}$$

where

$$S_c(\theta) = \frac{2\pi}{\Gamma} \int_o^\infty y \, \Omega(y) \, J_o\left(2ky \sin\frac{\theta}{2}\right) dy \tag{2.22}$$

Also

$$p_s = ip_i e^{ik|\vec{x}|} \frac{\Gamma k \delta\left(\vec{\lambda} \cdot \vec{t}\right)}{2a_\infty |\vec{x}|} \cos\theta \cot\frac{\theta}{2} S_c(\theta) \tag{2.23}$$

which result is the three-dimensional analog of the scattering formula (3.23) in Reference 1.

2) Horseshoe Vortex

To study the scattering of engine noise by lifting surfaces it is of interest to consider the horseshoe vortex

$$\vec{\omega}_o = \Gamma \{-\vec{i} \, \delta(y+\ell) \, \delta(z) \, H(x) + \vec{i} \, \delta(y-\ell) \, \delta(z) \, H(x) + \vec{j} \, \delta(x) \, \delta(z) \, H(\ell^2 - y^2)\} \tag{2.24}$$

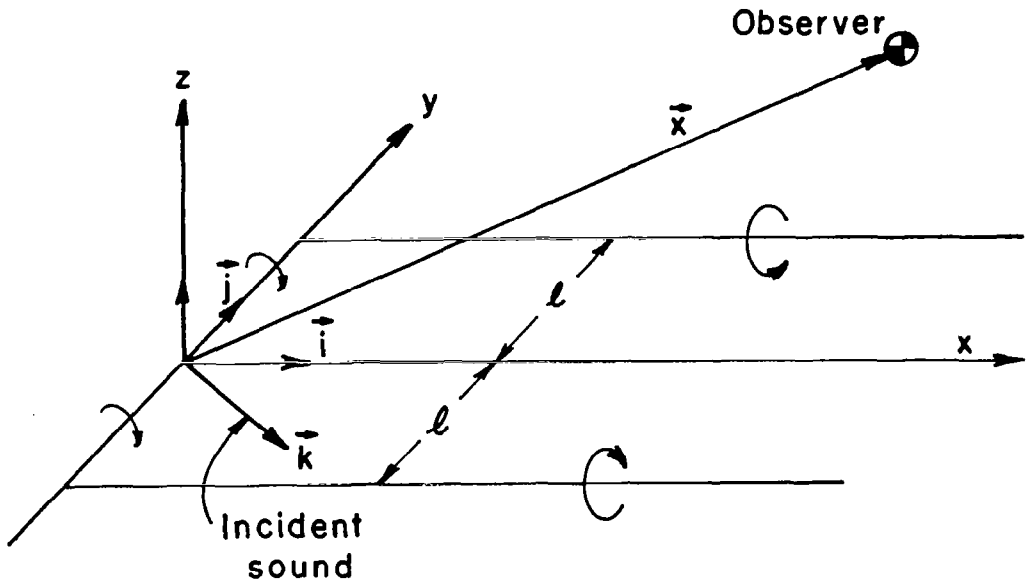

and using (2.17)

$$\vec{\omega}_o^* = \Gamma \left[-\vec{i}\, \frac{2 \sin (\vec{\lambda}\cdot\vec{j})\ell}{\vec{\lambda}\cdot\vec{i}} + \vec{j}\, \frac{2 \sin (\vec{\lambda}\cdot\vec{j})\ell}{\vec{\lambda}\cdot\vec{j}} \right]$$

$$= 2\Gamma \frac{(\vec{i}\times\vec{j})\times\vec{\lambda}}{(\vec{\lambda}\cdot\vec{i})(\vec{\lambda}\cdot\vec{j})} \sin (\vec{\lambda}\cdot\vec{j})\,\ell \qquad (2.25)$$

Thus

$$p_s = ip_i e^{ik|\vec{x}|} \frac{\Gamma k}{\pi a_\infty |\vec{x}|} \frac{(\hat{x}\cdot\vec{k})(\hat{x}\times\vec{k})\cdot[(\vec{i}\times\vec{j})\times\vec{\lambda}]}{\lambda^2(\vec{\lambda}\cdot\vec{i})(\vec{\lambda}\cdot\vec{j})} \sin (\vec{\lambda}\cdot\vec{j})\,\ell \qquad (2.26)$$

with

$$\vec{\lambda} = k\,\hat{x} - \vec{k}$$

The last result could be used with the general formula (2.38) given below to study in detail the scattering of engine or airframe noise by the lifting vortices of a wing. An important parameter that must be small in all of the scattering formula is $\Gamma k/a_\infty$.

3) Ring - Vortex

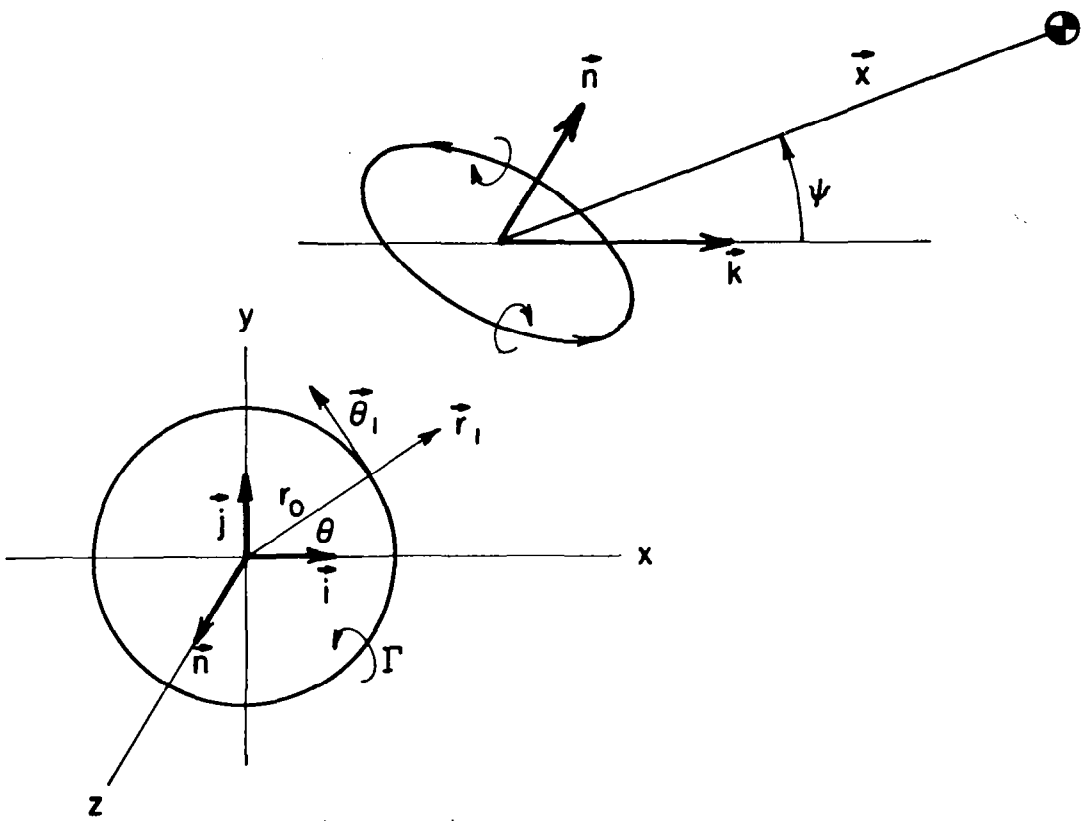

$$\vec{\omega}_o = \Gamma \, \vec{\theta}_1 \, \delta(z) \, \delta(r - r_o) \tag{2.27}$$

$$\begin{aligned} \vec{\theta}_1 &= -\vec{i} \sin\theta + \vec{j} \cos\theta \\ \vec{r}_1 &= \vec{i} \cos\theta + \vec{j} \sin\theta \end{aligned} \tag{2.28}$$

In the integral (2.17), suppose that the projection of $\vec{\lambda}$ on the plane of the vortex ring is aligned with the x-axis in the above sketch. Then

$$\vec{\lambda} \cdot \vec{y} = r_o \, \vec{\lambda} \cdot \vec{i} \cos\theta \tag{2.29}$$

and

$$\vec{\omega}_o^* = \Gamma r_o \int_o^{2\pi} e^{-ir_o \vec{\lambda} \cdot \vec{i} \cos\theta} (-\vec{i} \sin\theta + \vec{j} \cos\theta) \, d\theta \tag{2.30}$$

The first term in the integral is zero and the second reduces to a standard Bessel function. Thus

$$\vec{\omega}_o^* = -2\pi i\, r_o\, \Gamma\, \vec{j}\, J_1(r_o \vec{\lambda}\cdot\vec{i}) \tag{2.31}$$

and

$$p_s = p_i e^{ik|\vec{x}|}\, \frac{\Gamma k}{a_\infty}\, \frac{r_o}{|\vec{x}|}\, \frac{(\hat{x}\cdot\vec{k})(\hat{x}\times\vec{k})}{\lambda^2} \cdot \vec{j}\, J_1(r_o \vec{\lambda}\cdot i) \tag{2.32}$$

The vectors $\vec{i}$ and $\vec{j}$ can be expressed in terms of $\vec{\lambda}$ and $\vec{n}$ as follows:

$$\vec{i} = \frac{\vec{\lambda} - (\vec{\lambda}\cdot\vec{n})\vec{n}}{\sqrt{\lambda^2 - (\vec{\lambda}\cdot\vec{n})^2}}$$

$$\vec{j} = \vec{n} \times \vec{i} \tag{2.33}$$

An interesting special case of the foregoing result is when $\vec{n}$ and $\vec{k}$ are parallel. For then

$$p_s = p_i e^{ik|\vec{x}|}\, \frac{\Gamma k}{2a_\infty}\, \frac{r_o}{|\vec{x}|}\, \cos\psi\, \cot\frac{\psi}{2}\, J_1(kr_o \sin\psi) \tag{2.34}$$

which result should be compared with Eq. (2.23). The basic directivity is the same as that for an infinitely long vortex filament, although the intensity is not singular in the forward scattering direction. The basic directivity is plotted in Figure 2.1 for a compact ring ($kr_o << 1$). Note the strong but nonsingular forward scattering.

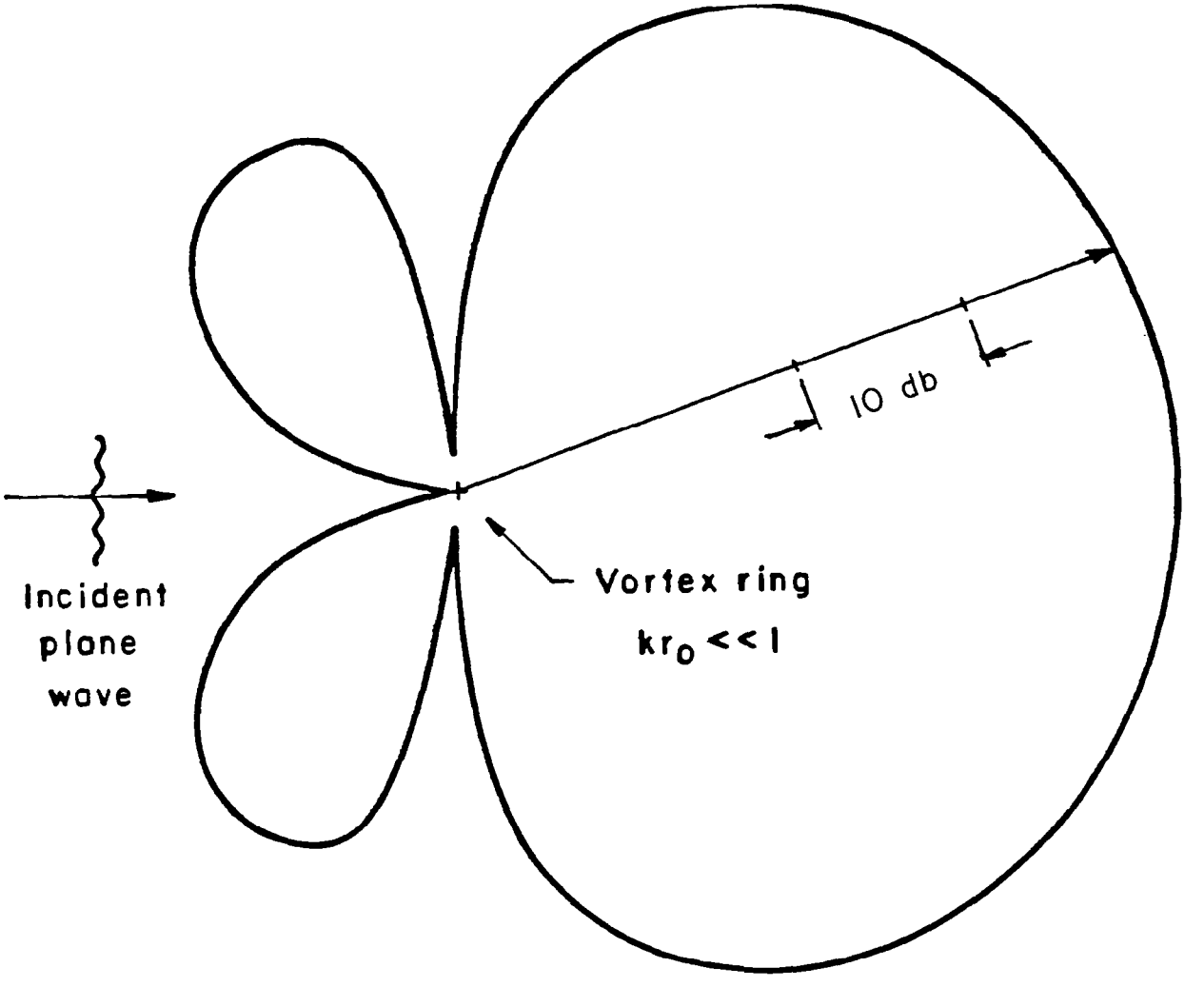

Figure 2.1 - Scattering of plane waves by a vortex ring, see Eq. (2.34).

4) Jet or Wake (Top Hat Vorticity)

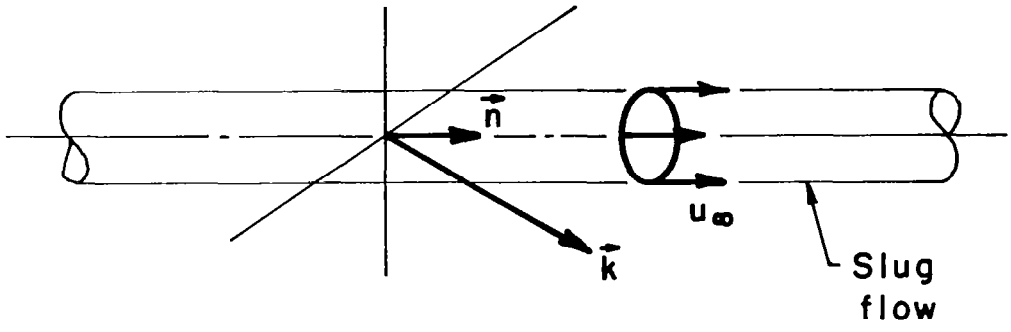

$$\vec{\omega}_o = \Gamma\ \vec{\theta}_1\ \delta(r - r_o) \tag{2.35}$$

By analogy with (2.27) and (2.29)

$$\vec{\omega}_o^* = -2\pi i\, r_o \Gamma\ \delta(\vec{\lambda}\cdot\vec{n})\ \vec{j}\ J_1(r_o\vec{\lambda}\cdot\vec{i}) \tag{2.36}$$

The pattern of the scattered sound is identical to that of the single vortex ring [see Eq. (2.32)]. This result suggests that a suitable distribution of fixed vortex rings would be a good model for calculating the scattering effect of a jet or wake.

The scattering formula (2.16) can easily be generalized for an arbitrary source pressure field expressed in terms of its plane wave components; i.e.,

$$p_i(\vec{x}) = \frac{1}{(2\pi)^3}\int e^{i\vec{\alpha}\cdot\vec{x}}\, p_i^*(\vec{\alpha})\, d\vec{\alpha} \tag{2.37}$$

Then

$$p_s = \frac{ike^{ik|\vec{x}|}}{(2\pi)^4 a_\infty |\vec{x}|}\int d\vec{\alpha}\ p_i^*(\vec{\alpha})\ \frac{(\hat{x}\cdot\vec{\alpha})(\hat{x}x\vec{\alpha})}{|k\hat{x} - \vec{\alpha}|^2}\cdot\vec{\omega}_o^*(k\hat{x} - \vec{\alpha}) \tag{2.38}$$

a rather neat Parseval type integral for the scattered sound field.

III. REVIEW OF DISCRETE VORTEX NOISE THEORY

Consider the motion of N two-dimensional point vortices of strength Γ_n with vector positions denoted by x_n (see Figure 3.1). The vortices move in the field of some arbitrary external flow $\vec{V}(\vec{x},t)$. The equations of motion of the vortices are

$$\dot{\vec{x}}_n = \sum_{m=1}^{N}{}' \gamma_n \vec{D}\left(\vec{x}_{nm}\right) + \vec{V}\left(\vec{x}_n, t\right) \tag{3.1}$$

$$\gamma_n = \Gamma_n / 2\pi \tag{3.2}$$

$$\vec{x}_{nm} = \vec{x}_n - \vec{x}_m = -\vec{x}_{mn} \tag{3.3}$$

$$\vec{D}(\vec{y}) = \frac{\vec{k} x \vec{y}}{|\vec{y}|^2} \tag{3.4}$$

The prime on the summation in (3.1) means that the term $m = n$ is to be omitted.

To calculate the farfield acoustic pressure due to the vortex motion it is necessary to calculate the second and third time derivatives of the vortex positions. It is convenient to introduce Cartesian tensor notation. Then

$$\dot{x}_n^i = \sum_{m=1}^{N}{}' \gamma_m D_{nm}^i + V_n^i \tag{3.5}$$

$$\ddot{x}_n^i = \sum_{m=1}^{N}{}' \gamma_m Q_{nm}^{ij} \dot{x}_{nm}^j + \mathring{V}_n^i \tag{3.6}$$

$$\dddot{x}_n^i = \sum_{m=1}^{N}{}' \gamma_m \left(Q_{nm}^{ij} \ddot{x}_{nm}^j + T_{nm}^{ijk} \dot{x}_{nm}^j \dot{x}_{nm}^k \right) + \mathring{\mathring{V}}_n^i \tag{3.7}$$

where

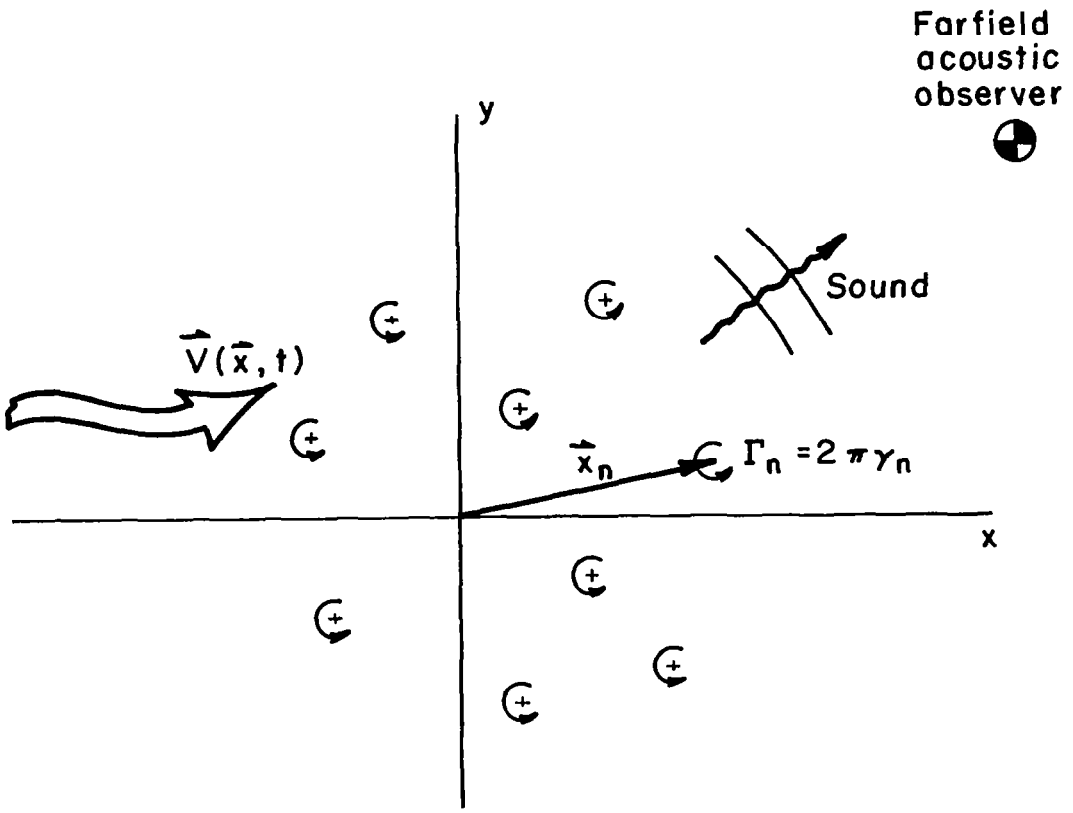

Figure 3.1 - Two-dimensional vortices in an external flow.

$$D^i(\vec{y}) = \frac{\check{y}^i}{R}$$

$$Q^{ij}(\vec{y}) = \frac{1}{R^2}\left(\varepsilon_{ij} - 2\check{y}^i\hat{y}^j\right)$$

$$T^{ijk}(\vec{y}) = -\frac{2}{R^3}\left(\varepsilon_{ij}\hat{y}^k + \varepsilon_{ik}\hat{y}^j + \check{y}^i\delta_{jk} - 4\check{y}^i\hat{y}^j\hat{y}^k\right) \tag{3.8}$$

$$\vec{y} = \left(y_1, y_2\right) \quad , \quad R = |\vec{y}|$$

$$\hat{y}^i = \frac{y^i}{R} \quad , \quad \check{y}^i = \varepsilon_{ij}\hat{y}^j$$

$$\varepsilon_{ij} = \begin{bmatrix} 0 & -1 \\ 1 & 0 \end{bmatrix} \quad , \quad \delta_{ij} = \begin{bmatrix} 1 & 0 \\ 0 & 1 \end{bmatrix} \tag{3.9}$$

Also

$$\begin{aligned} \overset{\circ}{V}{}^i_n &= V^i_{n,t} + V^{i,j}_n \dot{x}^j_n \\ \overset{\circ\circ}{V}{}^i_n &= V^i_{n,tt} + 2V^{i,j}_{n,t}\dot{x}^j_n + V^{i,j}_n \ddot{x}^j_n + V^{i,jk}_n \dot{x}^j_n \dot{x}^k_n \end{aligned} \tag{3.10}$$

with

$$\begin{aligned} V^i_n &= V^i\left(\vec{x}_{n,t}\right) \\ V^{i,j}_n &= \frac{\partial V^i_n}{\partial x^j_n} \quad , \quad V^i_{n,t} = \frac{\partial V^i_n}{\partial t} \end{aligned} \tag{3.11}$$

Note further that the tensor functions (3.8) can be expressed as follows in terms of the two Cartesian components of their argument:

$$D^1 = -y_2/R^2 \quad , \quad D^2 = y_1/R^2 \tag{3.12}$$

$$\begin{aligned} Q^{11} &= -Q^{22} = 2y_1y_2/R^4 \\ Q^{12} &= Q^{21} = \left(y_2^2 - y_1^2\right)/R^4 \end{aligned} \tag{3.13}$$

$$\begin{aligned} T^{111} &= -T^{122} = -T^{212} = -T^{221} = \frac{2y_2}{R^4}\left(1 - \frac{4y_1^2}{R^2}\right) \\ T^{222} &= -T^{112} = -T^{121} = -T^{211} = -\frac{2y_1}{R^4}\left(1 - \frac{4y_2^2}{R^2}\right) \end{aligned} \tag{3.14}$$

The above formulae are particularly convenient for evaluating the sound field.

For simplicity the sound field is evaluated for a compact array of vortices. The wave length must be much greater (factor of 15) than the maximum distance between pairs of vortices. In Reference 1, it was shown that in the compact limit all acoustic theories give the same answer for the radiated sound, at least for the spinning vortex pair. Furthermore, the most simple theory to apply is the formulation of Powell (Ref. 4) as developed by Hardin (Ref. 5). For these reasons the Powell-Hardin formulation is used in the following discussion.

In the Powell-Hardin theory for two-dimensional vortices, the three-dimensional sound field is calculated for a finite segment of the vortices . It is easy to show for a vortex pair (the proof is omitted here) that the angular pattern of the radiated sound is the same for the two- and three-dimensional sound calculations. Only the farfield decay rates differ; i.e.,

$$\begin{aligned} |p| &\sim \frac{1}{\sqrt{r}} \quad \text{2-D} \\ &\sim \frac{1}{r} \quad \text{3-D} \end{aligned} \tag{3.15}$$

The three-dimensional calculation is much more straightforward and is used in the following development.

The farfield sound pressure is given by the formula

$$p \cong -\frac{\rho_\infty}{4\pi a_\infty^2}\frac{x^i x^j}{|\vec{x}|^3}\left[\frac{\partial^2}{\partial t^2}\int y_i L_j \, d\vec{y}\right]^* \tag{3.16}$$

where the asterisk means that the expression in brackets is evaluated at the retarded time

$$t^* = t - |\vec{x}|/a_\infty \tag{3.17}$$

Also

$$\vec{L} = -\vec{u}\times\vec{\omega} \tag{3.18}$$

is the Coriolis acceleration. To apply (3.16) to an array of two-dimensional vortices, the integration is carried out over a segment of length L. The integration is over the plane of the vortices and the farfield is evaluated in the same plane. For a finite collection of two-dimensional vortices

$$\omega = \sum_{n=1}^{N} \Gamma_n \delta(\vec{x} - \vec{x}_n) \tag{3.19}$$

and the formula (3.16) reduces to

$$p = \frac{\rho_\infty L}{2a^2|\vec{x}|}\hat{d}_i \check{d}_j \sum_{n=1}^{N} \gamma_n \left[\frac{d^2}{dt^2}\left(x_n^i \dot{x}_n^j\right)\right]^* \tag{3.20}$$

where

$$\hat{d}_i = \frac{x_i}{|\vec{x}|}$$

$$\check{d}_i = \varepsilon_{ij}\hat{d}_j \tag{3.21}$$

The need for second and third time derivatives of $\vec{x}_n$ is evident from (3.20).

To evaluate the spectrum of the farfield pressure, a finite record length, T, is assumed, and the Fourier transform is calculated by standard FFT techniques (Ref. 6). The result is

$$S(\omega) = \sum_{n=-\infty}^{\infty} S_n(\omega_n)\,\delta(\omega - \omega_n) \tag{3.22}$$

where

$$\omega_o = 2\pi/T \quad , \quad \omega_n = n\,\omega_o$$

$$S_n = 2\pi |A_n|^2$$

$$A_n = \frac{1}{K} \sum_{k=1}^{K} e^{-\frac{in(k-1)2\pi}{K}} p_k \tag{3.23}$$

$$p_k = p\left(\frac{2\pi}{\omega_o} \cdot \frac{k-1}{K}\right)$$

The autocorrelation of the pressure can be calculated from the expression

$$R(\tau) = \frac{1}{2T} \int_{-T}^{T} p\,(t - \tau)\,p\,(t)\,dt$$

$$= A_o^2 + 2\sum_{n=1}^{\infty} |A_n|^2 \cos n\,\omega_o\,\tau \tag{3.24}$$

In the numerical results, emphasis is placed on the calculation of the pressure from (3.20) and the spectral coefficients S_n.

The purpose of the foregoing analysis is to provide a simple means of calculating the enhancement or attenuation of noise produced by elementary vortex configurations in various flows. The important problem of the acoustic excitation of vortex flows is also amenable to treatment with the foregoing analysis. Numerical results for several specific problems are discussed in detail in Section IV. One particular example is of sufficient interest to warrant further analysis; i.e., the problem of two vortices in a shear flow.

Referring to Figure 3.2, the equations of motion are

$$\begin{aligned} \dot{\vec{x}}_1 &= \gamma_2 \vec{D}_{12} + \vec{i}\, U'\left(\vec{j} \cdot \vec{x}_1\right) \\ \dot{\vec{x}}_2 &= \gamma_1 \vec{D}_{21} + \vec{i}\, U'\left(\vec{j} \cdot \vec{x}_2\right) \end{aligned} \tag{3.25}$$

Recall that γ is used to denote the vortex strength Γ divided by 2π. Introduce center of vorticity and relative position coordinates as follows:

$$\begin{aligned} \vec{x} &= \left(\gamma_1 \vec{x}_1 + \gamma_2 \vec{x}_2\right)/\gamma \\ \vec{r} &= \vec{x}_1 - \vec{x}_2 \\ \gamma &= \gamma_1 + \gamma_2 \end{aligned} \tag{3.26}$$

Then

$$\begin{aligned} \dot{\vec{x}} &= \vec{i}\, U' \vec{j} \cdot \vec{x} \\ \dot{\vec{r}} &= \gamma \vec{D}(\vec{r}) + \vec{i}\, U'(\vec{j} \cdot \vec{r}) \end{aligned} \tag{3.27}$$

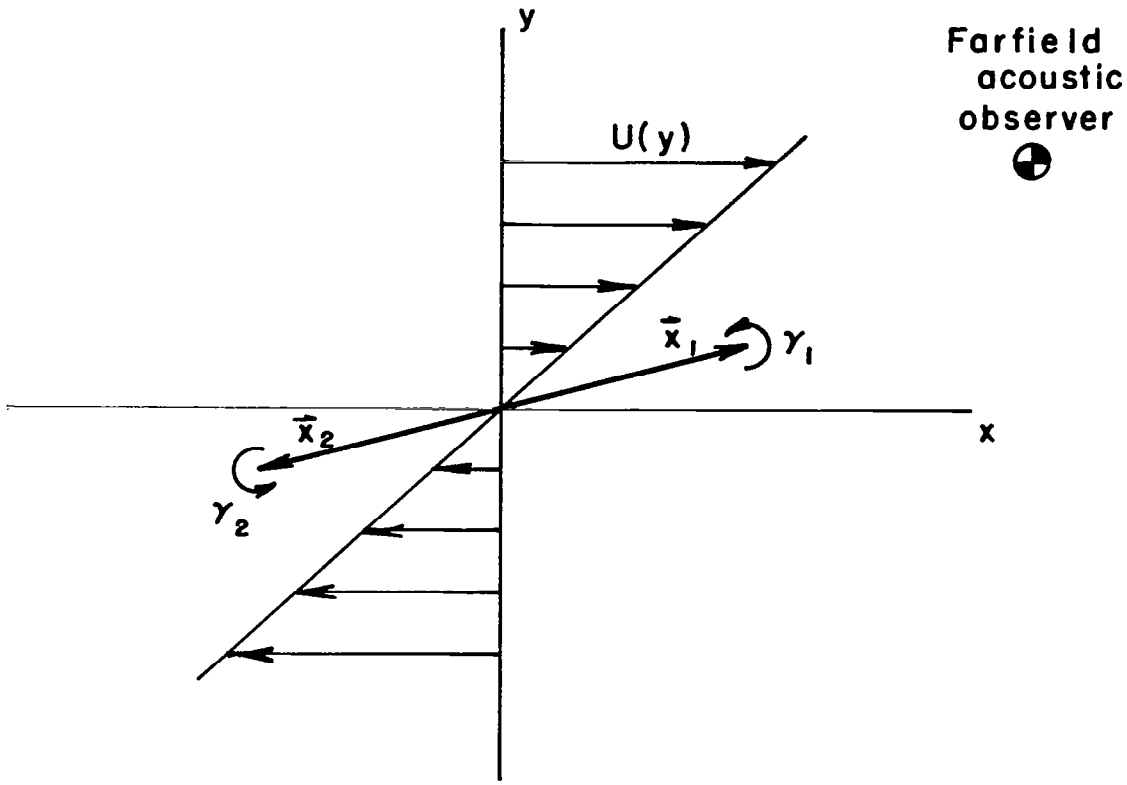

Figure 3.2 - Corotating vortex pair in a linear shear flow.

Assume that the center of vorticity is initially at the origin. Then the first of Eqs. (3.27) implies that $\vec{x}(t)$ is zero for all time. The relative motion of the vortex pair is expressed in terms of its Cartesian components as follows:

$$\dot{x} = -\frac{\gamma y}{r^2} + U'y$$

$$\dot{y} = \frac{\gamma x}{r^2} \qquad (3.28)$$

$$\vec{r} = (x,y) \quad , \quad r = |\vec{r}|$$

It is straightforward to solve for the trajectory of relative vortex motion and the period of rotation in the case of a closed orbit. The results are, for the trajectory:

$$r^2 = r_o^2 \, e^{\frac{U'}{\gamma}(y^2 - y_o^2)} \tag{3.29}$$

where r_o , y_o are the initial conditions. The period of rotation is

$$T = 4\left(\frac{r_o^2}{\gamma}\right)\delta \int_0^{\pi/2} \frac{e^{\lambda\delta^2\sin^2\theta}\cos\theta}{\left(e^{\lambda\delta^2\sin^2\theta} - \delta^2\sin^2\theta\right)^{1/2}} \, d\theta \tag{3.30}$$

where

$$\lambda = \frac{\ell n \, \delta^2}{\delta^2} \quad , \quad 0 < \delta < \sqrt{e}$$

$$= U' r_o^2/\gamma \tag{3.31}$$

For $\delta > \sqrt{e}$ or $\lambda > 1/e$, the relative motion of the pair is unbounded. When $\delta = 1$ $(\lambda = 0)$, the applied shear is zero and the orbit is circular with a period $\pi r_o^2/2\gamma$.

Typical trajectories of the pair are plotted in Figure 3.3 for various values of λ . The corresponding period of rotation T is noted for each bound trajectory. For positive shear $\lambda > 0$ the vortices are slowed down in their orbit which becomes elongated along the y-axis. For negative shear the opposite effect occurs and the orbit is flattened. A complete discussion of the noise generated by the sheared vortex configuration is given in Section IV.

IV. NUMERICAL CALCULATIONS OF VORTEX NOISE

With the general theory of the preceding section, it is possible to conduct numerical experiments of various noise producing flows. It is not the intent of this section to attempt a direct simulation of complex flows as others have done (e.g., see Refs. 7, 8). Rather, it is intended to illustrate specific noise enhancement mechanisms. The examples chosen are elementary, but the results are very illuminating and permit one to extrapolate (at least qualitatively) to more complicated situations. The results presented are of two main types. The first set of

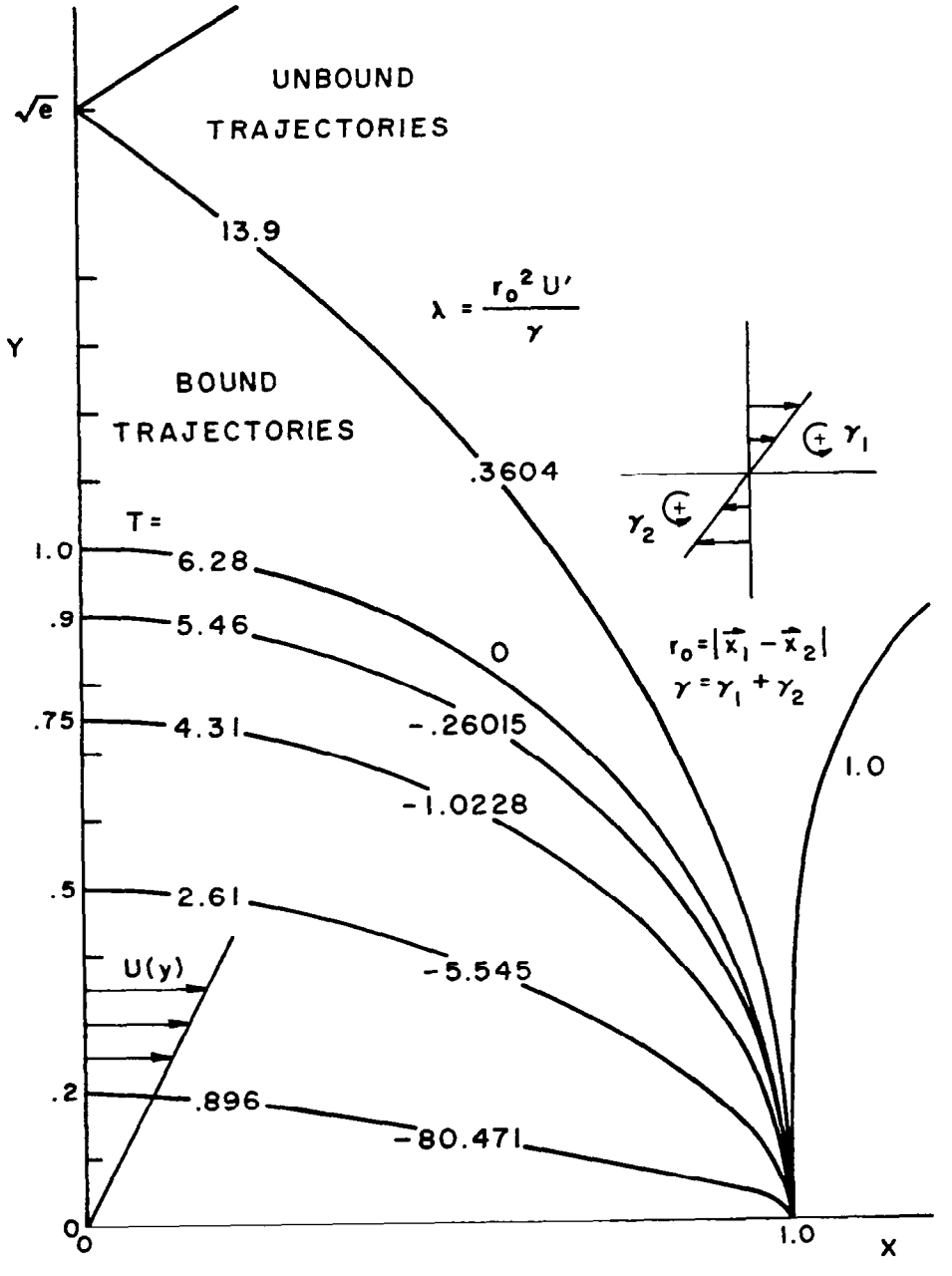

Figure 3.3 - Typical trajectories of a vortex pair in a linear shear flow.

results illustrates how the noise of an elementary vortex pair is changed when the pair is subjected to various external flows. The second set of results focuses on the problem of acoustic stimulation and reradiation of elementary vortex flows.

The spinning vortex pair is considered to be the basic fluid flow model of an aerodynamic noise producing element. A complete analysis of the vortex pair was given in Reference 1. For low speed pairs ($M < .1$) the noise produced is equivalent to that of a single compact quadruple. The sound produced is essentially a pure tone with a frequency twice the rotation rate of the pair. The two-dimensional sound power scales as M^7. With the three-dimensional analysis of the preceding section, the power scales as M^8. Even though the overall sound is quadrupole in nature, a detailed calculation of $D\mathcal{H}/Dt$ shows that the radiated sound is the end result of a more complex monopole structure (see Figure 4.2 of Reference 1). For more energetic pairs ($M > .1$) the sound power radiated is significantly less than that calculated with the compact M^7 scaling low (see Figure 4.3 of Reference 1).

It is interesting to ask how the sound of a simple vortex pair changes with the relative strength of the two vortices. The answer is presented in Figure 4.1. The sum of the strengths (divided by 2π) of the two vortices is .4 m^2/sec and the relative spacing is .05 m giving a radiation frequency of 50 Hz. The ratio γ_1/γ_2 is varied from minus one to plus one. For positive ratios the pair of equal strength radiates the most noise. For large negative ratios, the noise can be much greater than the pair of equal strength. For small positive and negative ratios the noise is significantly less than that of the pair of equal strength. For the remainder of this study the equal strength pair is used. For most of the pair calculations the vortex strength is .2 m^2/sec and the spacing is .05 m. The noise of the free pair is 31.7 db at a pure tone frequency of 50 Hz.

The first example of vortex noise enhancement is illustrated in Figure 4.2. The basic vortex pair is brought into the flow-field of a third large vortex with $\gamma_3 = 2$ m^2/sec. The acoustic observer is 10 m from the large vortex, and the ratio L/D was varied from 2.5 to ∞. The acoustic results for a free and fixed third vortex were virtually the same. This result indicates that the sound is a direct result of the small pair and its nonlinear interaction with the potential flowfield of the large vortex. The overall sound power versus the ratio L/D is presented in Table 4.1 for positive and negative sense of rotation of the central vortex. For positive rotation rates (i.e., all vortices with the same sign), the noise is enhanced significantly for $L/D \lesssim 7$. For negative rotation rates the noise is reduced for $L/D > 5$ and is then enhanced for closer spacing. The fundamental frequency of the small pair is not changed substantially

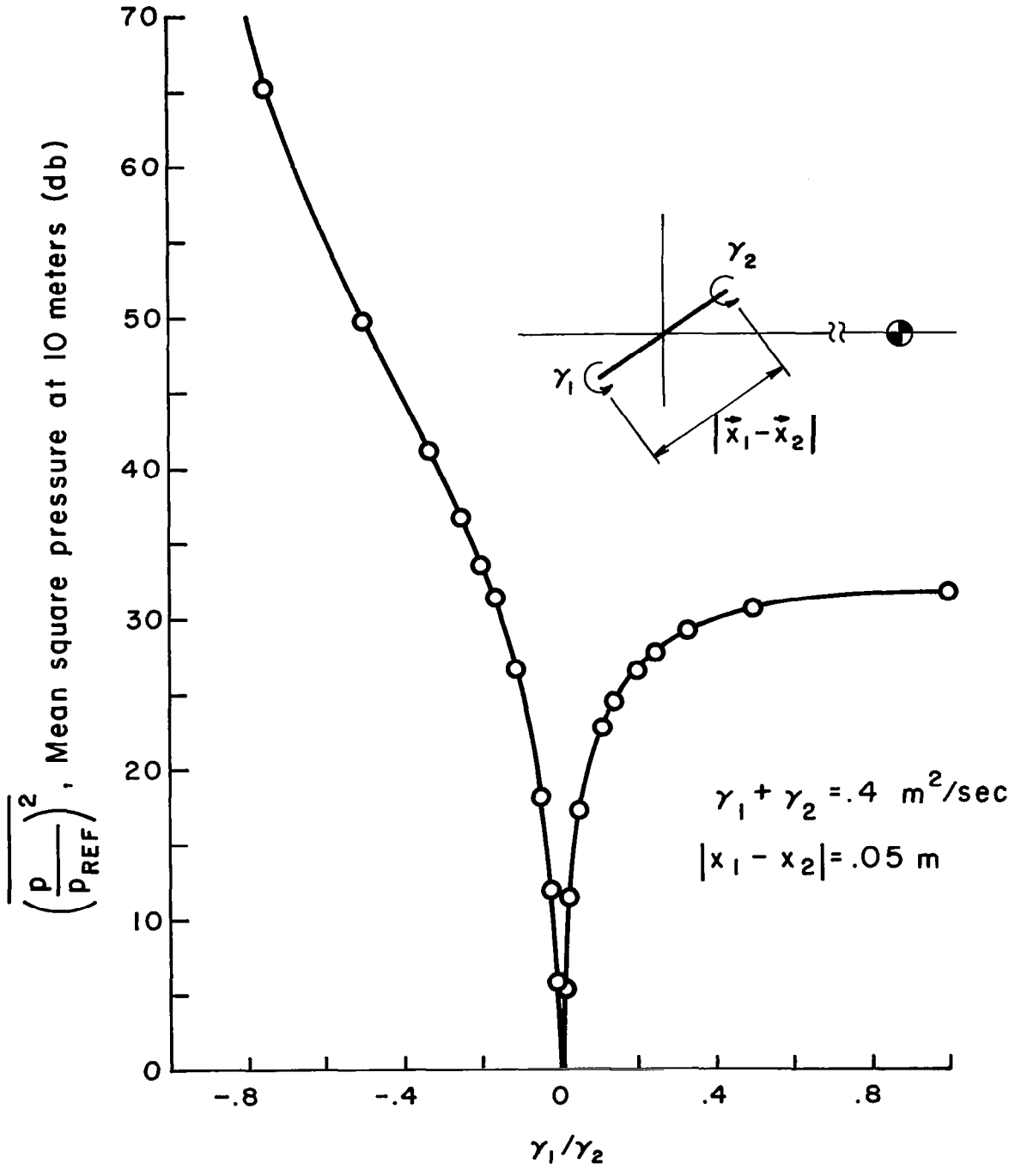

Figure 4.1 - Noise radiated by a vortex pair of unequal strength ($p_{ref} = 2 \times 10^{-5}$ N/m^2).

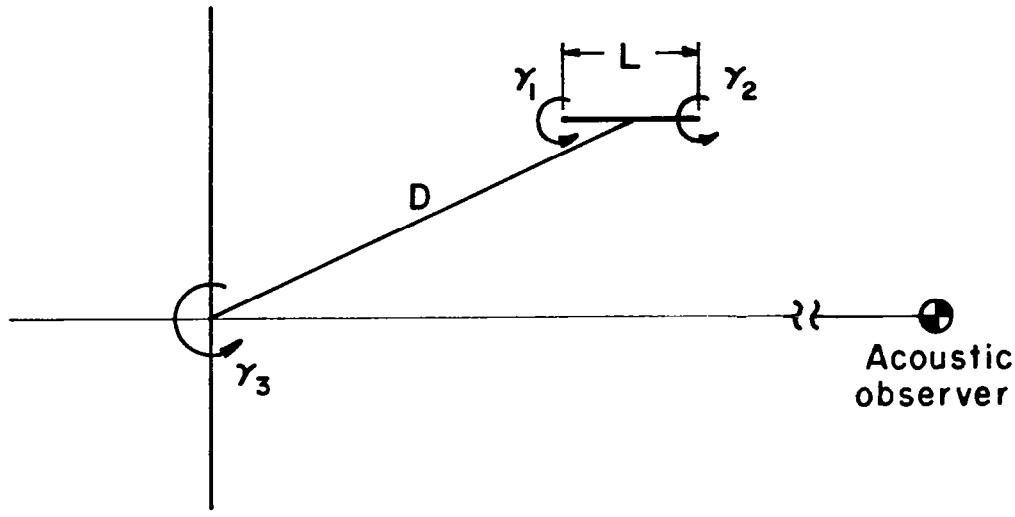

Figure 4.2 - Noise amplification by a potential flow.

TABLE 4.1 - OASPL OF A COROTATING AND COUNTER-ROTATING VORTEX PAIR IN THE FIELD OF A THIRD LARGE VORTEX

($\gamma_1 = \gamma_2 = .2$ m^2/sec, $\gamma_3 = \pm 2$ m^2/sec)

L/D	Corotating	Counter-Rotating
∞	31.7	31.7
20.00	31.9	31.5
10.00	32.7	31.0
7.50	33.7	30.6
5.00	37.9	31.7
3.75	44.8	37.6
2.50	60.2	50.6

for moderate amplifications because the flowfield is irrotational. On the other hand, the spectral content of the noise is significantly changed even for relatively large spacings. For example, in Figures 4.3 and 4.4 the trajectory, farfield pressure, and spectrum are presented for the ratio L/D = 10 . Note the strong harmonics in the spectrum as well as a very low frequency spike associated with the motion of the large vortex. This modulation can also be seen in the pressure trace. The presence of harmonics

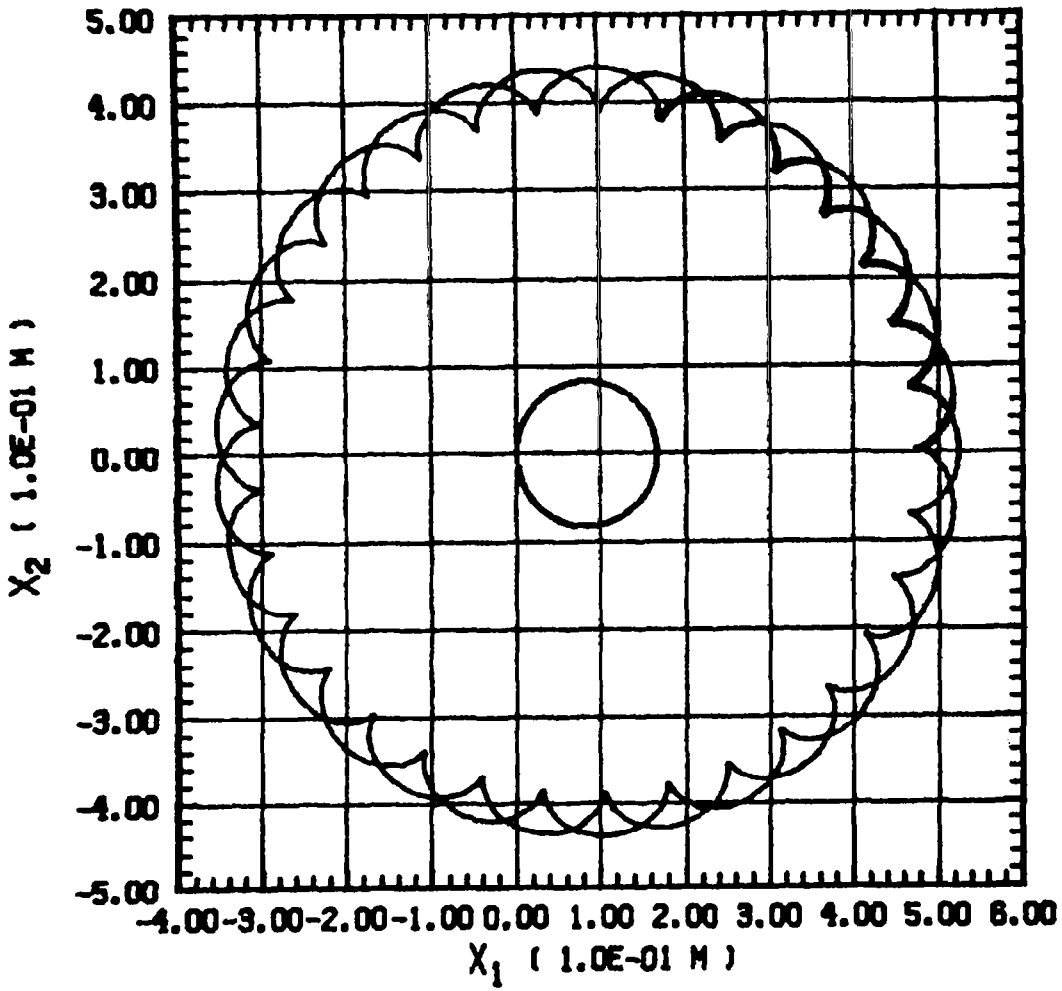

Figure 4.3 - Three vortex trajectories ($\gamma_1 = \gamma_2 = .2$ m^2/sec, $\gamma_3 = 2$ m^2/sec, L/D = 10.0 .

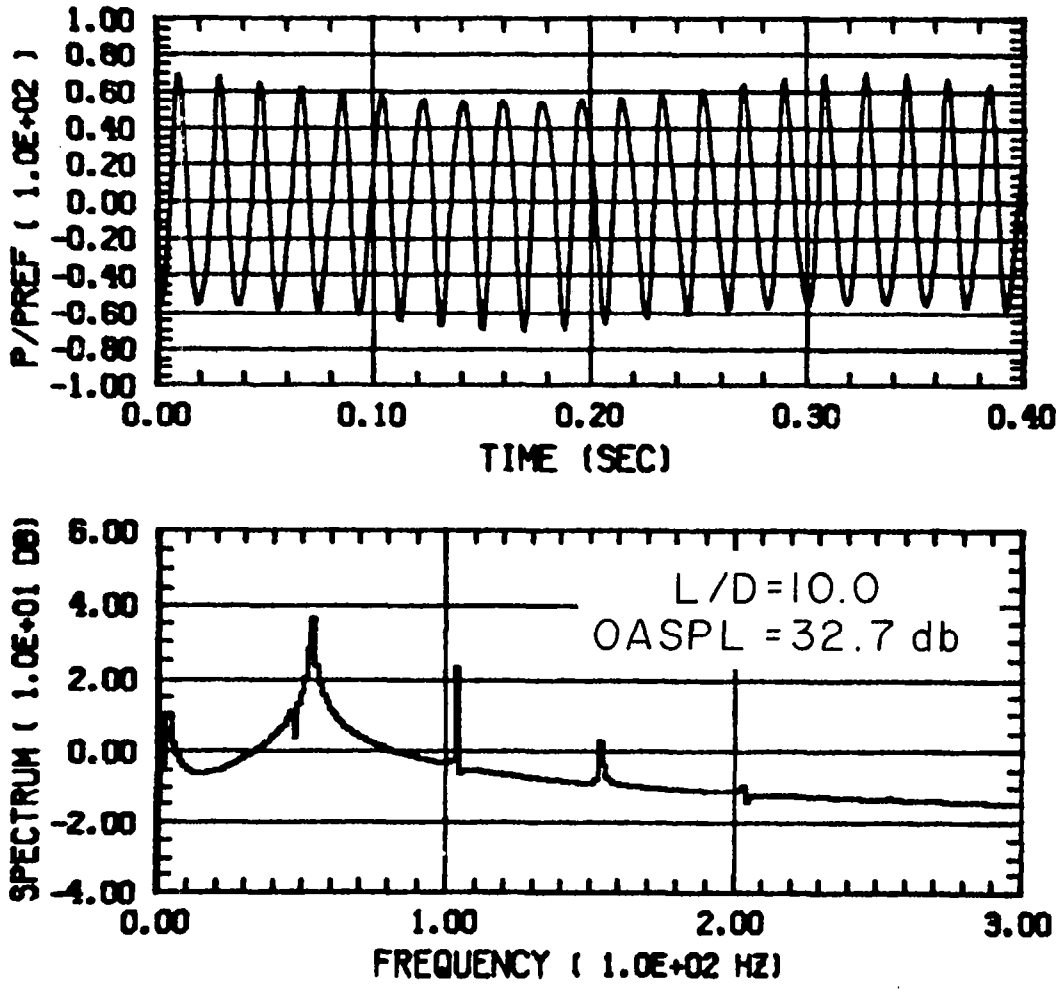

Figure 4.4 - Farfield pressure and spectrum of the basic vortex pair in the field of a third vortex ($\gamma_1 = \gamma_2 = .2$ m^2/sec, $\gamma_3 = 2$ m^2/sec, L/D = 10.0).

in the spectrum indicates that nonlinear distortion (acceleration) of the basic pair has occurred. The pressure trace and spectrum for $L/D = 5$ are given in Figure 4.5. The OASPL is up by 6 db over the free pair and the spectrum is very rich in harmonic content. For small vortex pairs with higher frequencies similar amplification results are obtained.

The foregoing results give a simple picture of the noise amplification that can result when turbulence is accelerated by a potential flow. A good practical example is the turbulence entrained into a vortex wake. The most highly concentrated wing vortices can be expected to be the most noisy during aircraft approach. It is expected that any technological advances that alleviate the wake hazard by redistributing the shed vorticity will also be beneficial in reducing airframe noise. Another practical illustration of the simple example is the free jet. Large discrete vortex structures emitted by a jet would entrain and amplify the small eddy motion of the noise producing turbulence. The noise enhancement mechanism would be alleviated by breaking up the larger structures as, for example, with a multitube noise suppressor.

In Section III, the analysis of the motion of two vortices spinning in a shear flow was given. The noise (OASPL) directivity for typical positive and negative shear is given in Table 4.2. For positive shear (opposite rotation sense to the vortices) the vortices are slowed down in their orbit and the noise is reduced. The noise pattern is essentially isotropic with a 3 db reduction at 90 degrees to the mean flow. For negative shear (same rotation sense as the vortices) the noise is enhanced with a slight 1.5 db increase at 90 degrees to the flow. The shear amplification is 4 to 6 db for $\lambda = -.125$, and the attenuation is -5 to -8 db for $\lambda = +.125$. For $\lambda = -.25$ the amplification is 7 to 9 db.

The pressure traces and noise spectra for $\lambda = \pm .125$ are given in Figures 4.6 and 4.7. The downward shift of the fundamental frequency ($\approx$33 Hz) for $\lambda = .125$ is a direct result of the increased orbital period. Conversely, the upward shift ($\approx$60 Hz) for $\lambda = -.125$ is due to the reduced orbital period. It is seen that much of the radiated noise in the presence of shear is in the higher frequency components. This is due to the nonlinear distortion of the vortex motion that is clearly evident in the pressure traces and the trajectories. For much larger shear values, the noise spectrum becomes very rich in pure tones superimposed on a broadband background. Typical results for $\lambda = -2.5$ are given in Figure 4.8. The noise is greater by some 30 db for this value of the shear. The noise at 90 degrees to the flow is 4 db greater than that in the flow direction.

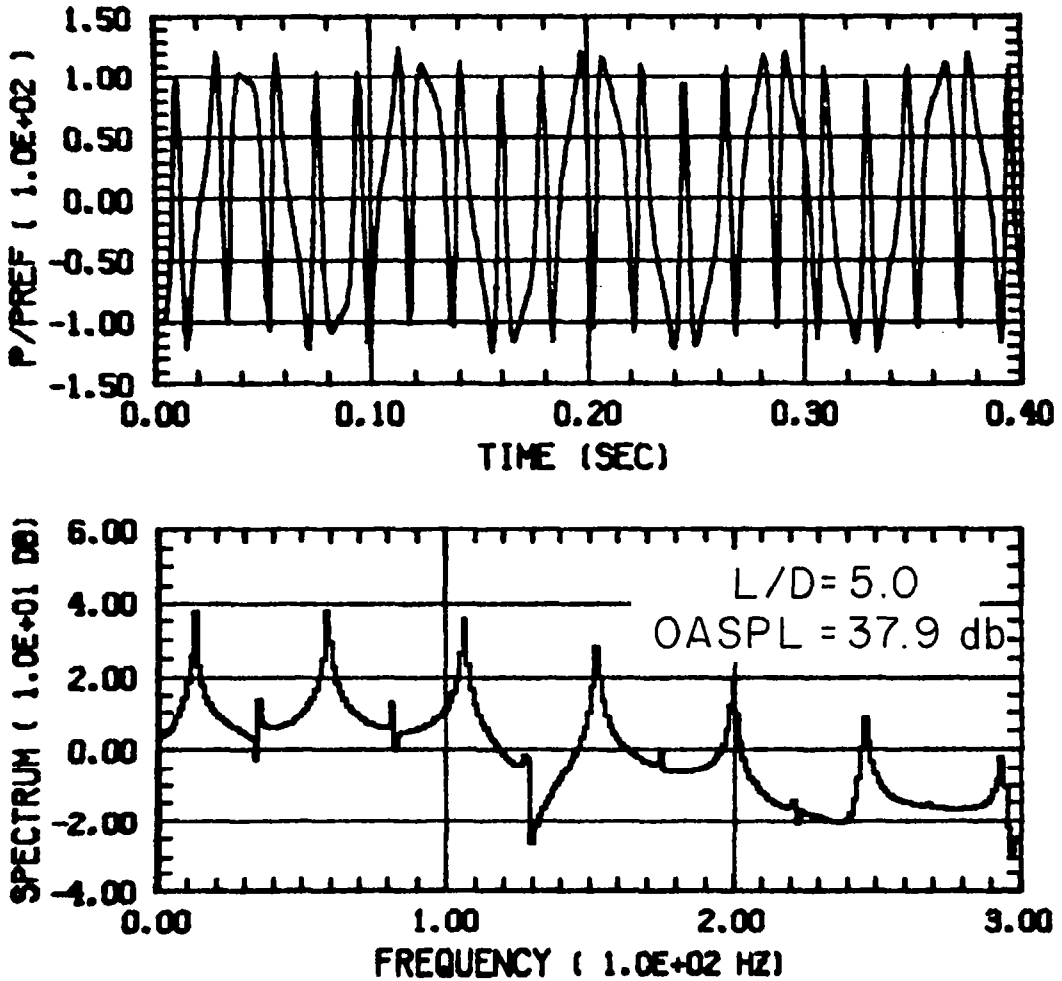

Figure 4.5 - Farfield pressure and spectrum of the basic vortex pair in the field of a third vortex ($\lambda_1 = \lambda_2 = .2$ m^2/sec, $\lambda_3 = 2$ m^2/sec, L/D = 5.0).

TABLE 4.2 - OASPL DIRECTIVITY FOR SPINNING VORTEX PAIR IN POSITIVE AND NEGATIVE SHEAR

Degrees	$\lambda = .125$	$\lambda = -.125$
0	27.0 db	35.7 db
22.5	26.8 db	36.0 db
45.0	26.0 db	36.6 db
67.5	24.7 db	37.0 db
90.0	24.1 db	37.2 db

The practical significance of shear amplification and attenuation of vortex noise is well known. Some of the elementary results thus obtained can be used to make some general inferences about jet noise. For example, the most obvious inference is that "reverse shear" is a good way to reduce the noise of a vortex pair and is therefore probably a good way to reduce jet noise. Coaxial noise suppressors are good examples of the beneficial use of reverse shear. The shear parameter λ is essentially the ratio of the mean shear rotation rate to the rotation frequency of the spinning vortex pair. The noise of high frequency pairs is much less affected by mean shear than are the low frequency pairs. Note, however, that for $\lambda = -.25$ the noise is increased by some 7 db. Thus, it is only the "very high" frequency pairs that are unaffected by shear. The inference is that mean negative shear would enhance the noise of a given turbulent flow over a wide frequency band. Only the noise of the very small high frequency eddies (that is, small to begin with) would be unaffected. With reverse shear, vortex pairs are destroyed for $\lambda > 1/e \simeq .36$ (see Figure 3.3). This result suggests that the low frequency "pair noise" mechanism can be virtually eliminated with a large reverse shear.

The last example of vortex-pair noise enhancement is illustrated in Figure 4.9. The rotating pair (basic noise = 31.7 db) is brought into the proximity of an infinite wall. The sound pressure level for various values of the ratios L/D is given in Table 4.3. The observer is on the wall far from the pair ($R = 10$ m, $\theta = 0$ degrees). For $L/D > 2$ the approximate 6 db noise increase is due to acoustic imaging. For closer spacings the noise is increased by more than 6 db because of the strong vortex interaction with the wall. Even for $L/D = 2$ the spectrum is changed with strong harmonics of the basic tone appearing (see Figure 4.10). For $L/D = 1$ the OASPL is greater by some 10 db.

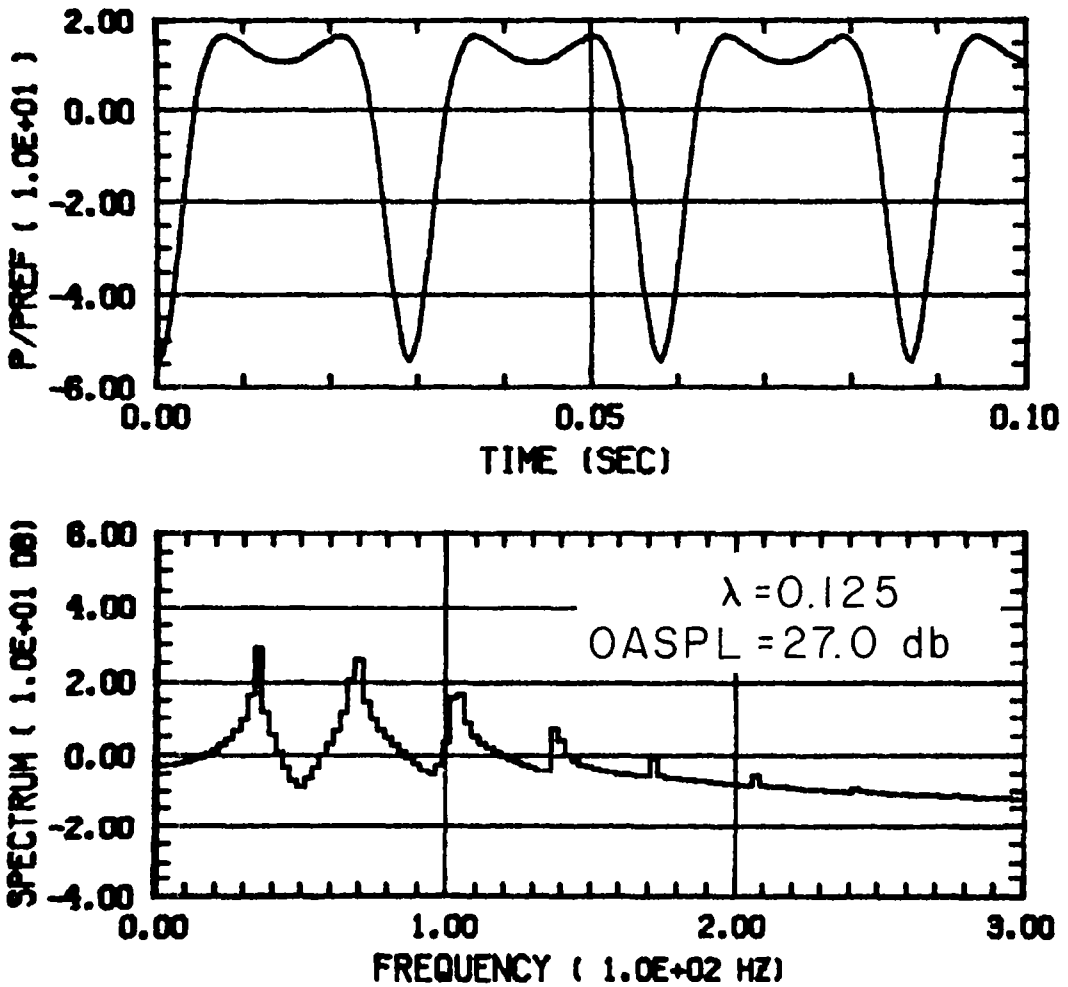

Figure 4.6 - Farfield pressure and spectrum of the basic vortex pair in a shear flow (λ = 0.125).

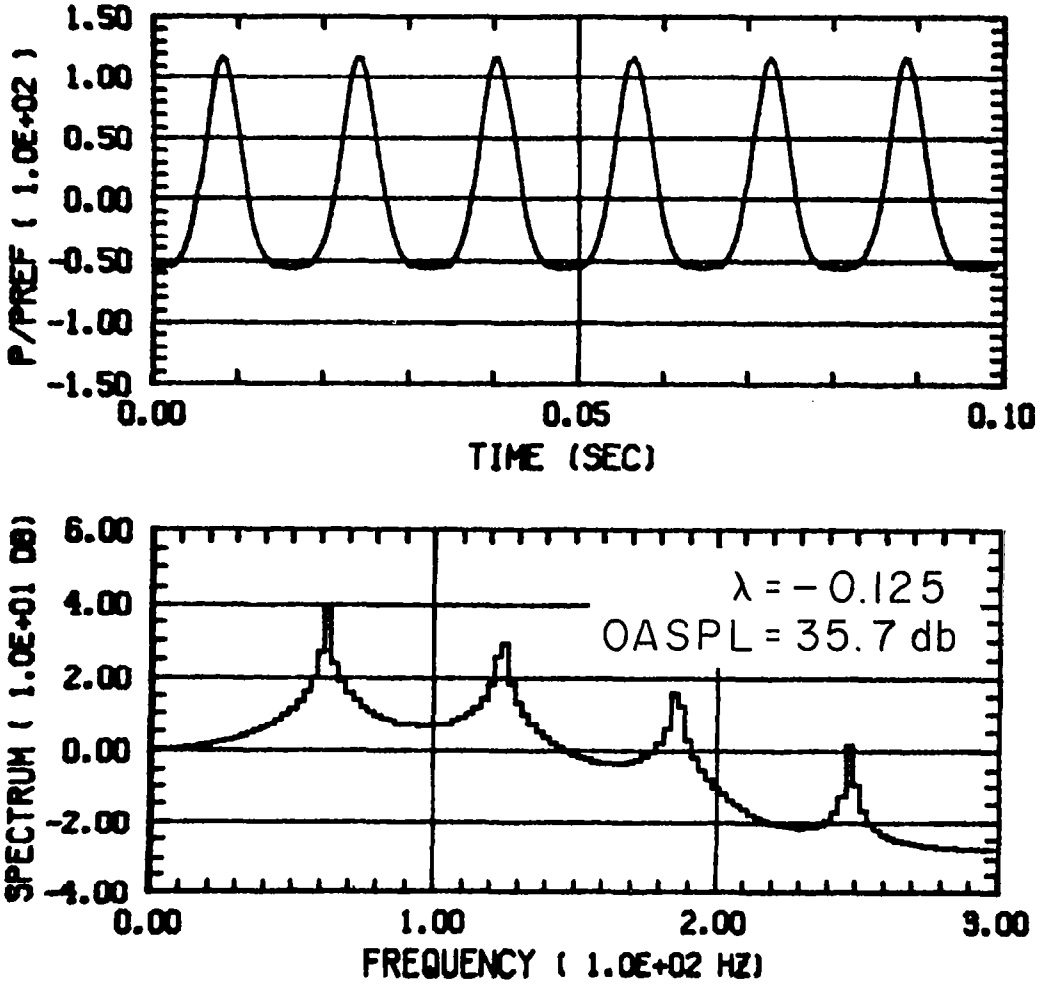

Figure 4.7 - Farfield pressure and spectrum of the basic vortex pair in a shear flow (λ = -0.125).

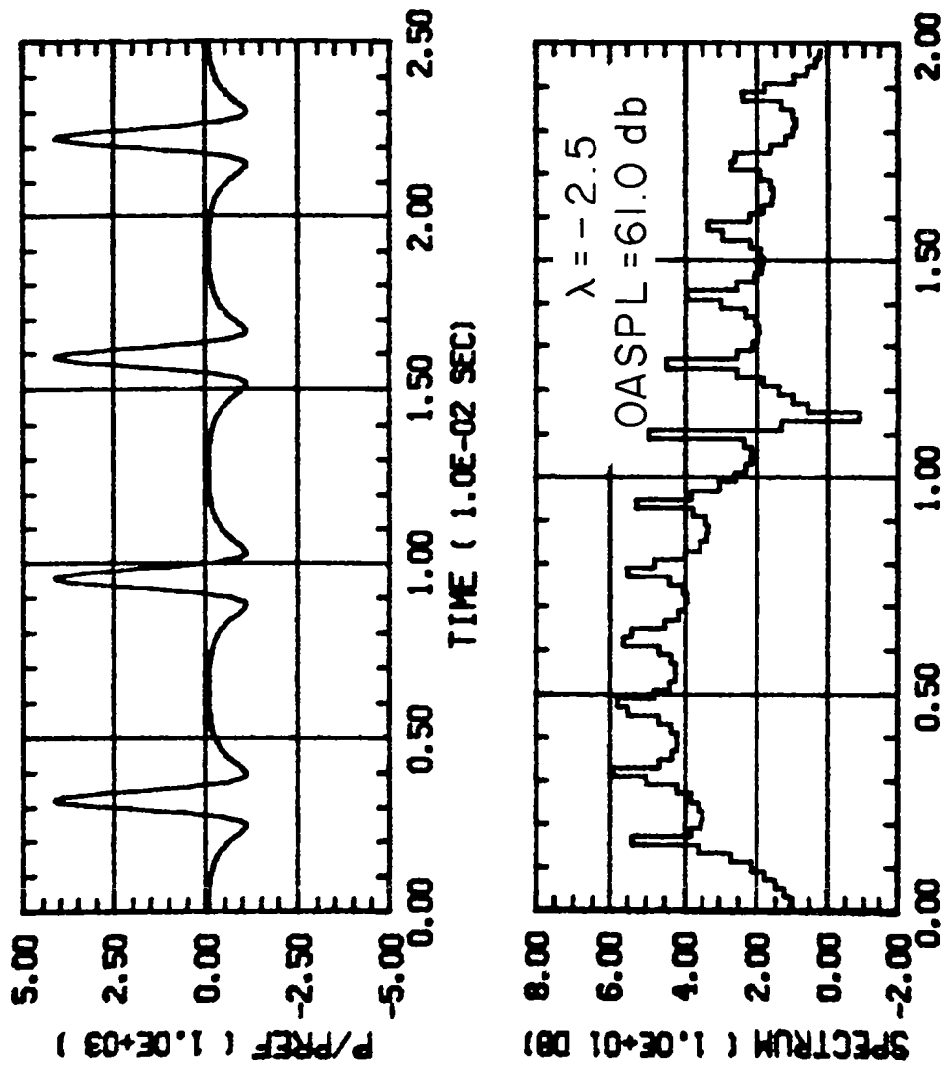

Figure 4.8 - Farfield pressure and spectrum of the basic vortex pair in a shear flow (λ = -2.5).

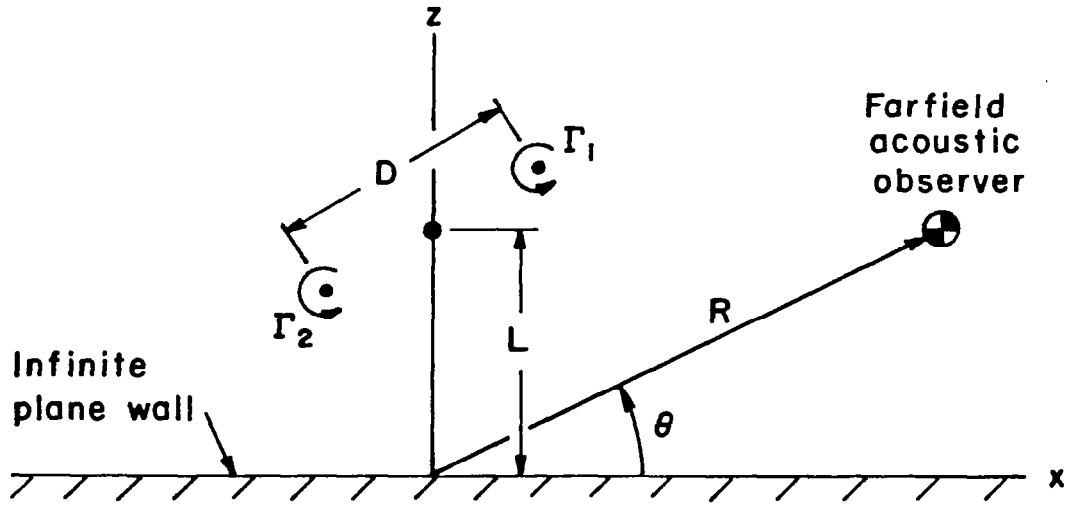

Figure 4.9 - Basic vortex pair near a plane wall.

TABLE 4.3 - OASPL OF THE BASIC PAIR NEAR A WALL

L/D	OASPL
8.0	37.7 db
4.0	37.8 db
2.0	38.4 db
1.5	39.0 db
1.0	41.2 db

The spectrum is very rich in harmonic content as evidenced in Figure 4.11. The directivity of the noise for L/D = 1 is plotted in Figure 4.12. The noise pattern is quadrupole-like with no noise radiated at 45 degrees to the wall. The effect of solid boundaries (in particular "edges") on simple vortex flows should be the subject of a further in-depth study of vortex noise.

An attempt was made to calculate the noise of a vortex pair in a stagnation point flow. The goal was to illustrate by simple example the enhancement of jet noise due to impingement on a solid surface. The computational difficulty is that the vortex pair is convected out of the stagnation region at an exponential rate. It is difficult, if not impossible, to isolate the noise

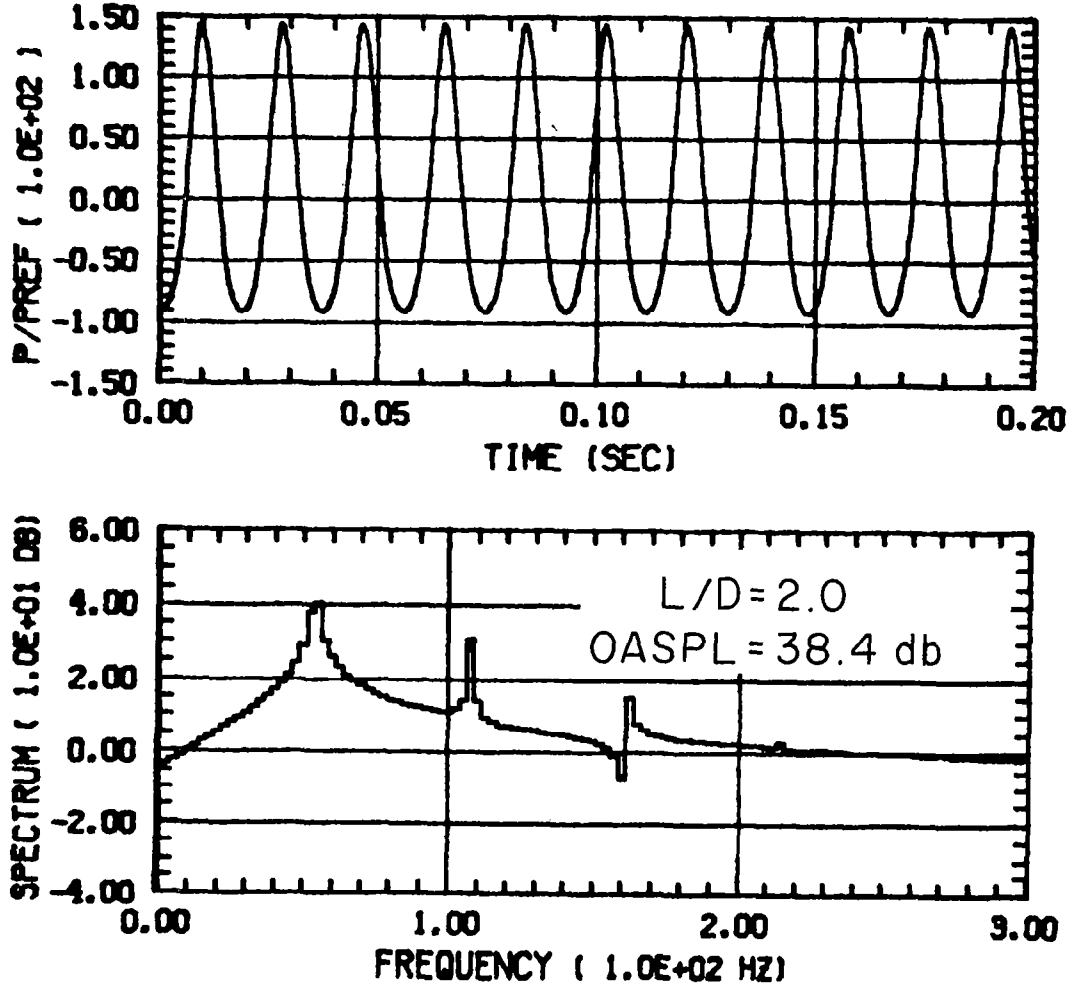

Figure 4.10 - Farfield pressure and spectrum of the basic pair near a wall (L/D = 2.0).

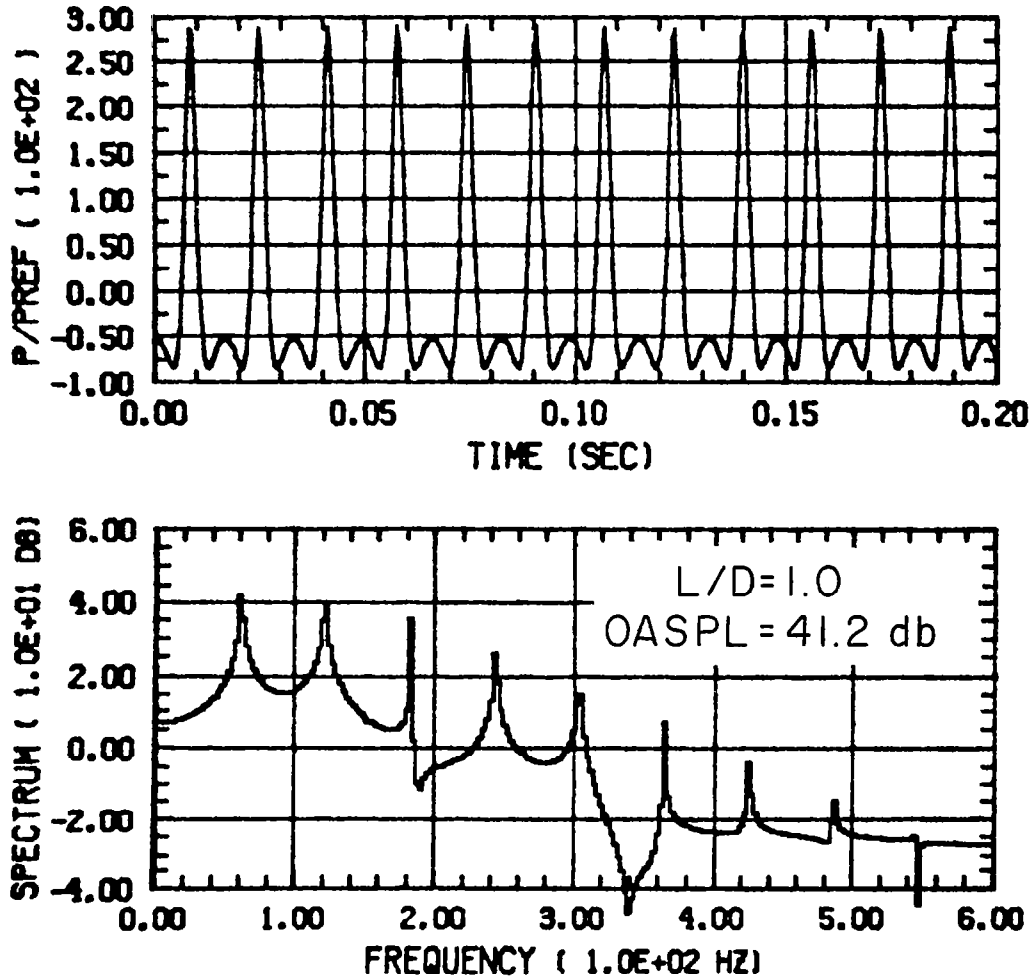

Figure 4.11 - Farfield pressure and spectrum of the basic pair near a wall (L/D = 1.0).

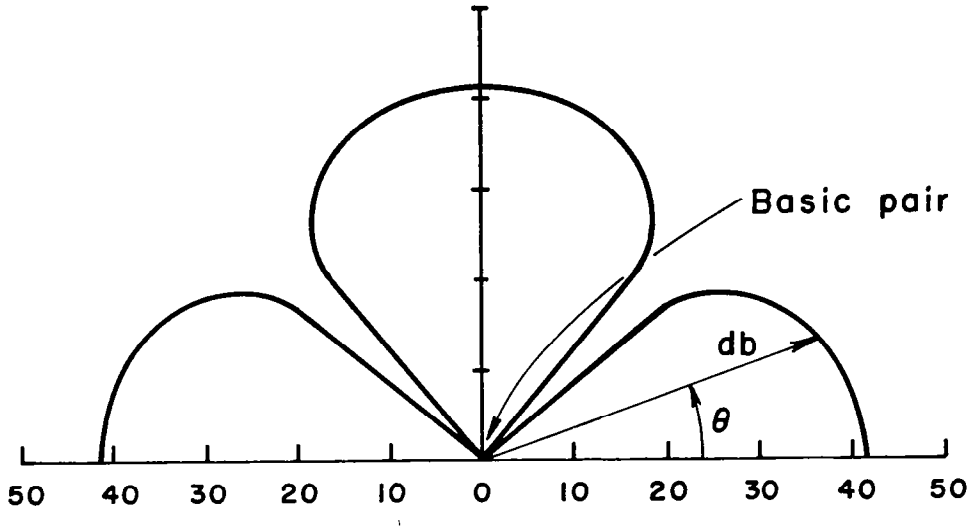

Figure 4.12 - OASPL directivity of basic vortex pair near a wall (L/D = 1.0).

due to a single rotating pair. To properly simulate the impingement problem it appears that a statistical sample of vortices with influx and outflux from a finite region near the stagnation point must be treated. From the other examples treated in this section, it is easy to conjecture that the highly curved flow near a stagnation point will result in an enhancement of vortex pair noise. See the related discussion in Reference 1, page 57.

In Reference 1, some preliminary work was done on the acoustic excitation of vortex flows. The motion of a vortex pair excited by an incident plane wave was calculated. It was shown that resonant excitation of the pair occurs when the frequency of the incident sound is nearly tuned to the pair acoustic radiation frequency. It was furthermore conjectured that the nearfield excitation would result in additional noise in the farfield. Direct calculation of the noise has shown that amplification and attenuation can occur.

For the basic pair (see p. 24), sound caused the vortex to become excited but no change in the radiated sound field resulted. For this case the Mach number of the vortex is about .01 and the wave length is about 300 times greater than the vortex spacing. The acoustic coupling is very weak. On the other hand, the results for a vortex pair that radiates a tone of 5000 Hz with a vortex Mach number of about 0.1 are shown in Figures 4.13 through 4.16. The pressure trace and spectrum of the unexcited pair are shown in Figure 4.13. The OASPL at 10 m is 111.7 db. The corresponding results for excitation frequencies 4800, 5000, and 5500 are shown in Figures 4.14 through 4.16. In each case,

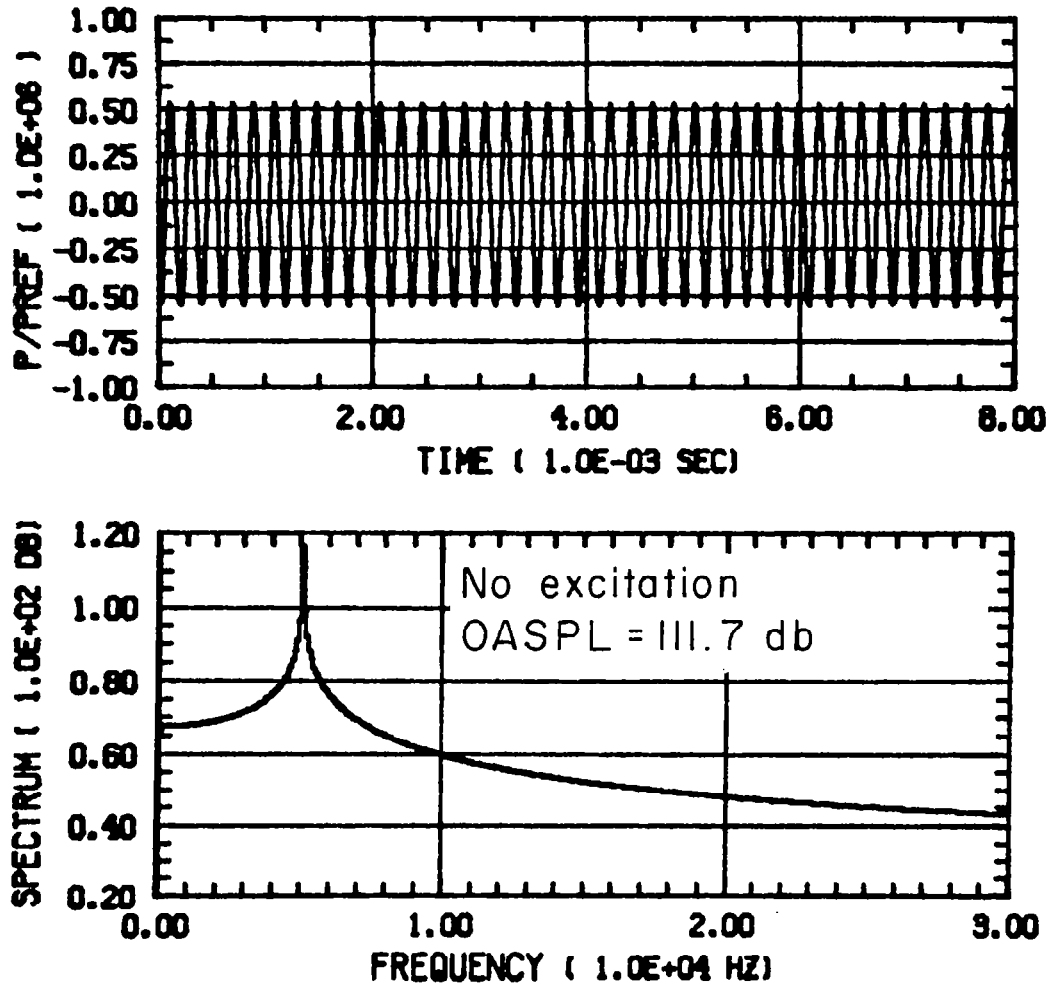

Figure 4.13 - Farfield pressure and spectrum of an unexcited vortex pair ($\gamma_1 = \gamma_2 = .2$ m^2/sec, $r_o = .005$ m).

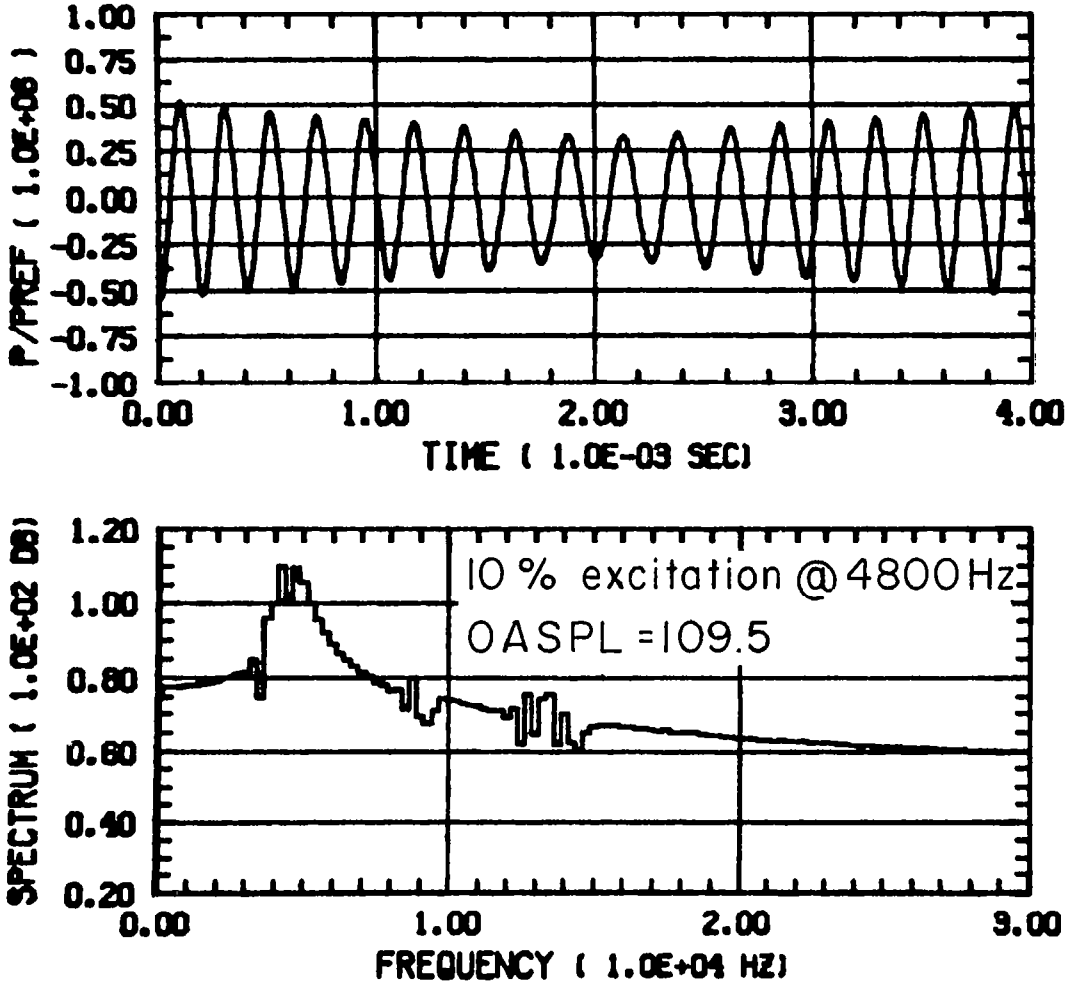

Figure 4.14 - Farfield pressure and spectrum of an excited vortex pair (ω_e = 4800 Hz).

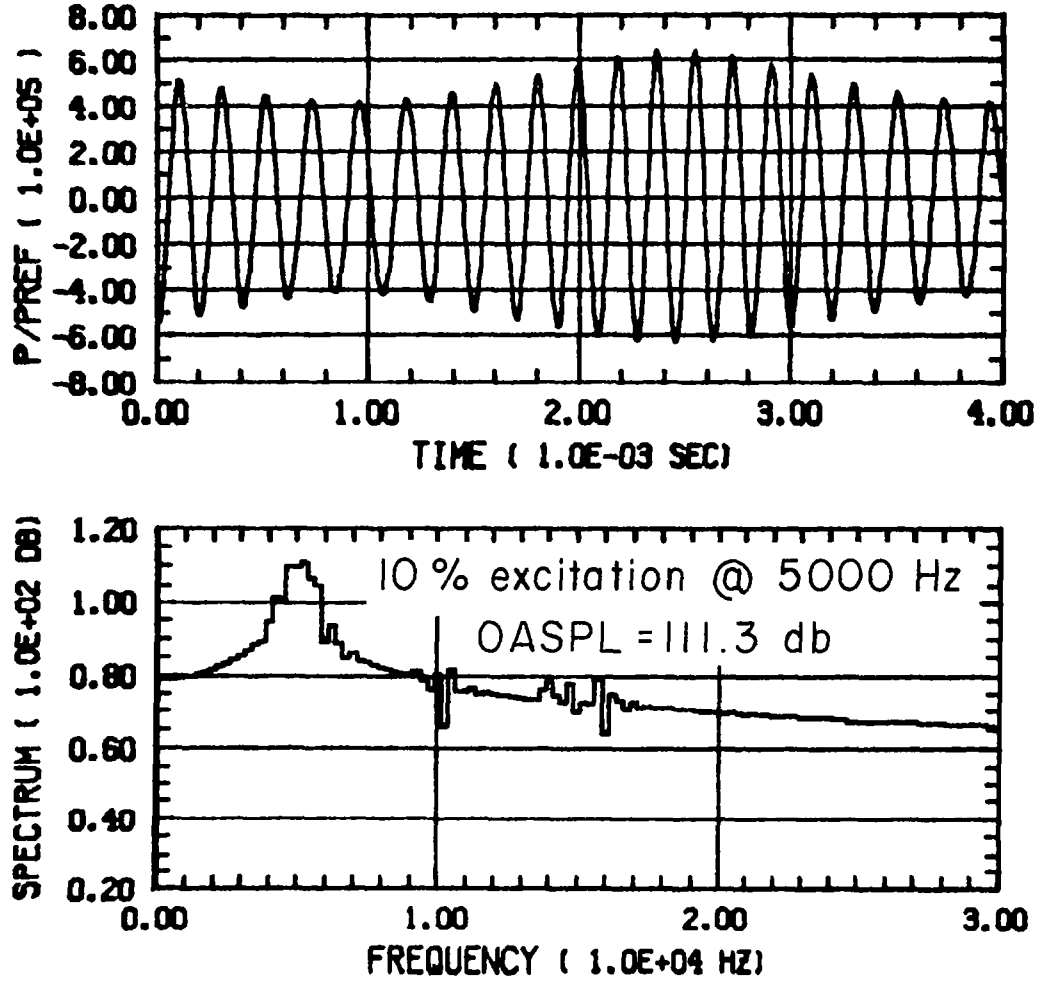

Figure 4.15 - Farfield pressure and spectrum of an excited vortex pair (ω_e = 5000 Hz).

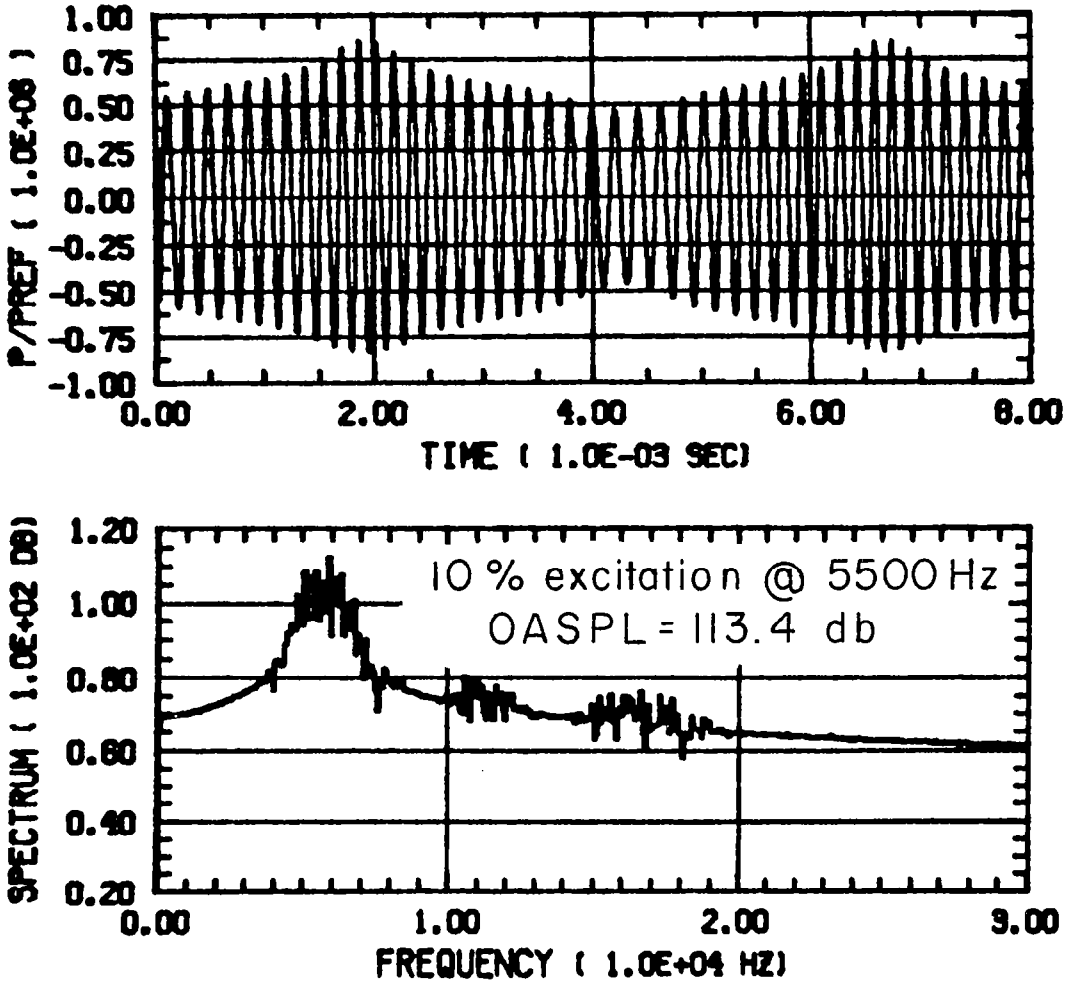

Figure 4.16 - Farfield pressure and spectrum of an excited vortex pair (ω_e = 5500 Hz).

the acoustic excitation level is approximately one tenth of the vortex Mach number or about .01. For an excitation frequency of 4800 Hz (Figure 4.13), the noise is attenuated by 2.2 db and for 5500 Hz (Figure 4.16), it is amplified by 1.7 db. At 5000 Hz (Figure 4.15), there is virtually no change in the radiated sound. Another interesting feature of the excited pair is that the unexcited pure tone is broadened by several hundred Hz. This frequency modulation is evident also in the pressure traces. Very little upper harmonic excitation occurs and the radiated sound pattern remains isotropic in all cases considered. The isotropic radiation pattern is a little surprising since the incident sound is unidirectional. One might expect more sound at 90 degrees where the resulting Coriolis force is a maximum. The mechanism of coupling is somewhat more subtle and depends on the relative motion of the pair.

An amplification or attenuation level of 2 db at ten percent excitation is significant and shows that a relatively simple unsteady free vortex flow is acoustically sensitive. By comparing Figures 4.13 through 4.16 with the plots of DH/Dt in Reference 1, Figures 5.6, 5.8, 5.10, it is seen that the farfield pressure is the virtual image of the nearfield DH/Dt . It should also be pointed out that no farfield effects are detected when the excitation frequency is substantially detuned. The phenomenon thus described depends on a frequency resonance, and the efficiency of the acoustic coupling depends on the ratio of wave length to vortex spacing.

The acoustic excitation of four vortices is illustrated in Figures 4.17 through 4.22. Two pairs of corotating vortices ($\gamma_1 = \gamma_2 = 2$ m^2/sec and $\gamma_3 = \gamma_4 = -.04$ m^2/sec) are considered. The large pair has a basic frequency of 1430 Hz, while the small pair frequency is 5430 Hz. The trajectories of the unexcited motion are plotted in Figure 4.17, and the spectrum is given in Figure 4.18a. The first two spectral peaks correspond to the basic pair frequencies.

In Figures 4.18b and 4.18c, the result of acoustic excitation at 1430 Hz is illustrated. The excitation velocity is ten percent of the maximum vortex velocity. The two spectra show the sensitivity of acoustic excitation to the phase of the source. At zero phase (see Figure 4.18b), the OASPL is slightly less (.2 db) than the unexcited case, while for the 135-degree phase the noise is greater by 2 db. The sensitivity to phase variation was noted in most cases of acoustic excitation. At the 135-degree phase, the noise in the second spectral peak is almost entirely suppressed while the low frequency tone is enhanced.

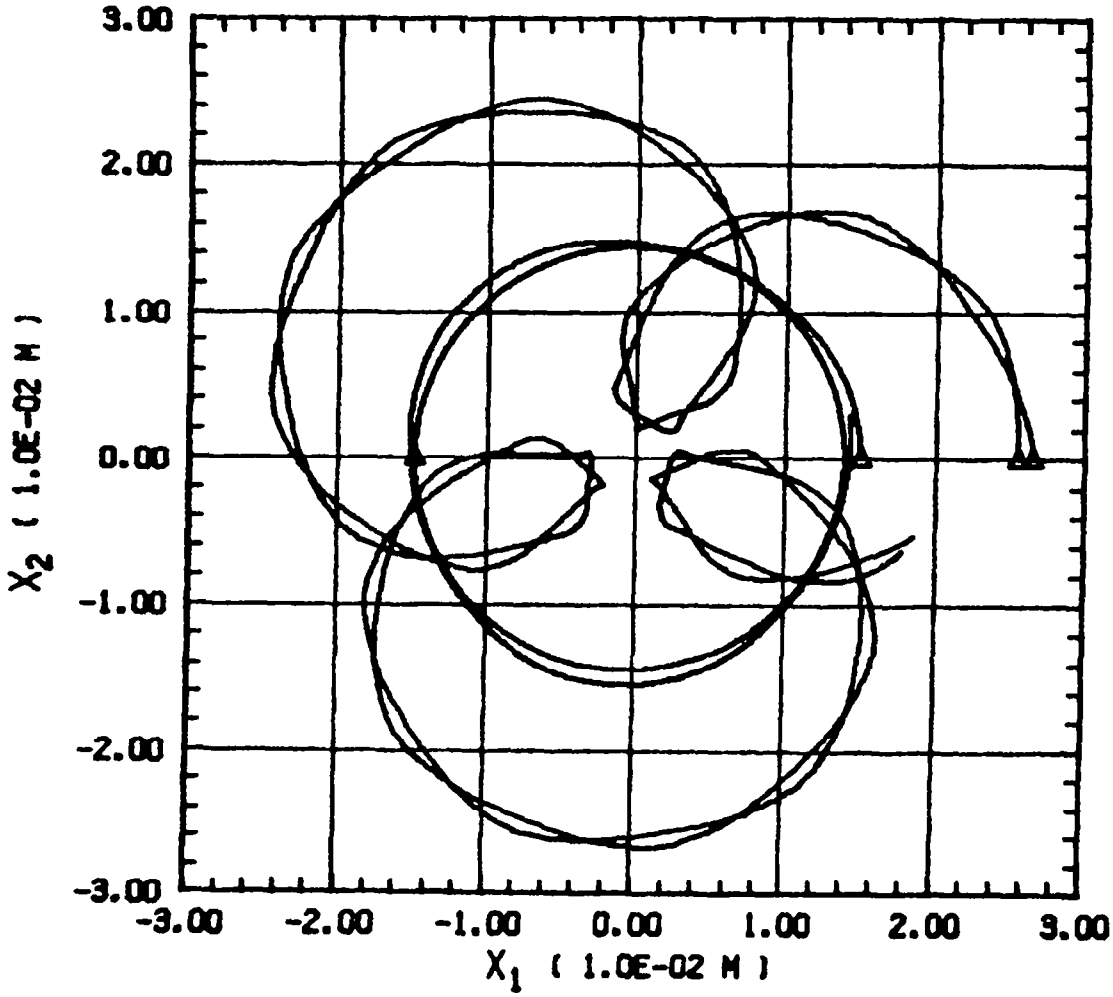

Figure 4.17 - Trajectories of four vortices;
$\gamma_1 = \gamma_2 = 2$ m^2/sec,
$\gamma_3 = \gamma_4 = -.04$ m^2/sec.

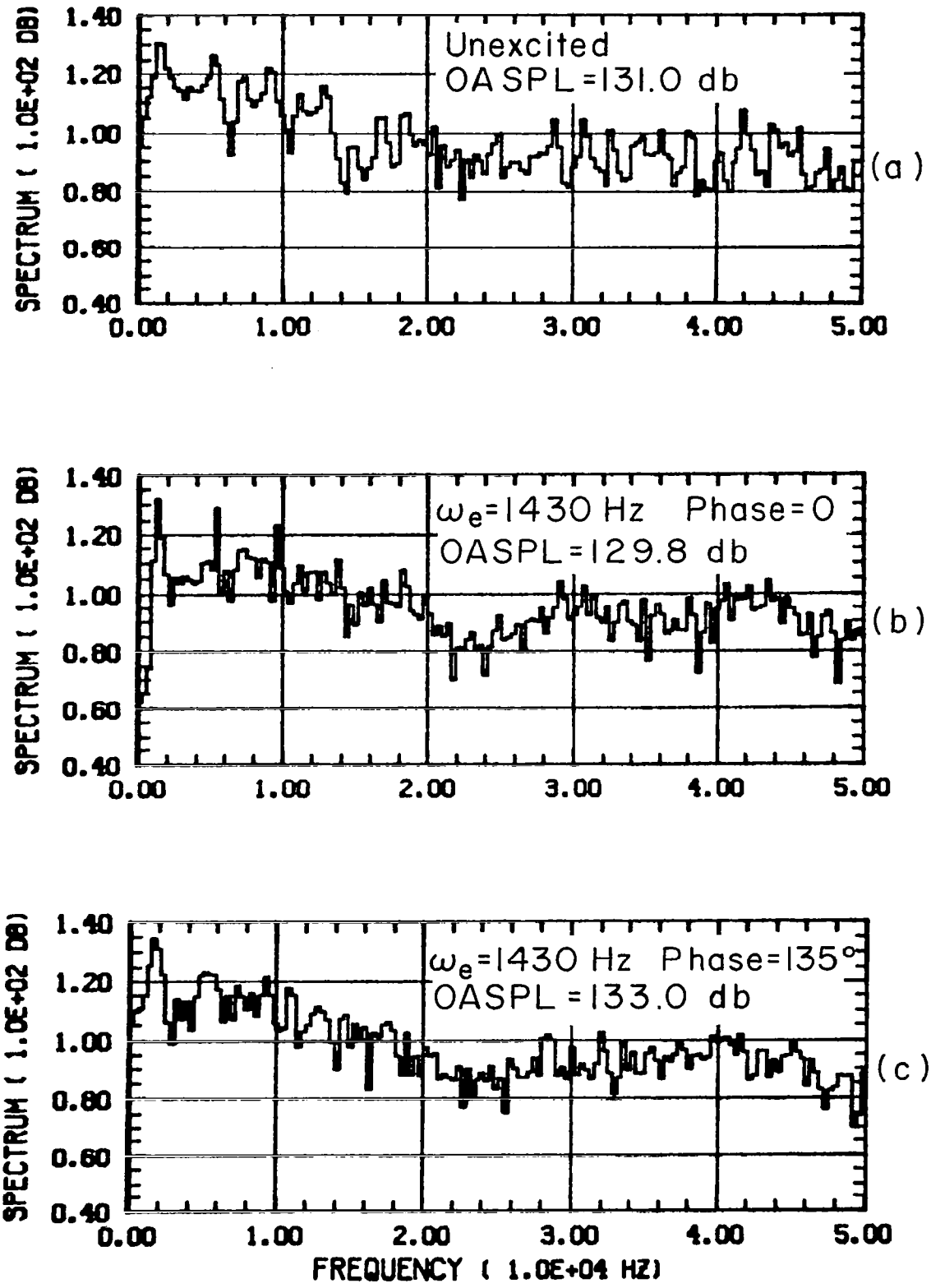

Figure 4.18 - Unexcited and excited spectra of four vortices; ω_e = 1430 Hz.

The results in Figure 4.19a, b, and c are also for the 135-degree phase with slight variations of the excitation frequency. The most noise enhancement occurs at 1480 Hz, and the high frequency noise is slightly suppressed. It was suspected earlier that the high frequency pair noise would generally be enhanced by the acoustic excitation of the low frequency pair. No evidence of this type of result was discovered for the four-vortex problem.

In Figure 4.20a, b, and c the spectra are given for acoustic excitation at three frequencies near the second spectral peak. The noise is enhanced by 3 db at 5450 Hz excitation (zero phase). It is evident from the spectra that the noise is increased in the frequency range above the excitation tone. Further evidence of acoustic excitation is presented in Figure 4.21a through f. The excitation is varied from 9000 to 9350 Hz (zero phase). The excitation is maximum at 9050 Hz with the increased noise spread over the octave band above the excitation frequency. This is the first indication of what might be construed as broadband amplification by a pure tone. However, the pressure field of four vortices has a very tonal character with no clearly defined broadband. The results for six vortices is much more illuminating.

The final set of results on acoustic excitation of vortex flows is for six vortices of equal strength (γ = .2 m^2/sec) that has the basic unexcited farfield spectrum shown in Figure 4.22. The noise has a typical broadband shape with a fairly broad spectral peak around 700 Hz. The spectrum also has a strong 200-Hz tone that is not very sensitive to acoustic excitation. The six-vortex array was scanned with a pure tone from zero to 2000 Hz. The excitation level is approximately ten percent of the maximum vortex velocity. The OASPL amplification results are given in Table 4.4. Amplification levels are relatively low for a tone below 400 Hz. The largest amplifications occur for tones just beyond the knee of the spectrum; i.e., 3.8 db at 750 Hz and 6.3 db at 1000 Hz. A large amplification, 4.4 db, is also obtained at an excitation frequency of 2000 Hz.

The spectra at the frequencies of largest amplification are given in Figures 4.23 through 4.26. For 750 and 1000 Hz it is seen by comparison with Figure 4.22 that the entire broadband spectrum is amplified. The excitation tone itself does not even show up in the spectrum. For an excitation frequency of 2000 Hz the tone is clearly evident in the spectrum and the amplification is over a wide band above and below the tone. These calculations are in qualitative agreement with recent experimental results on excited jet noise (Refs. 2, 3).

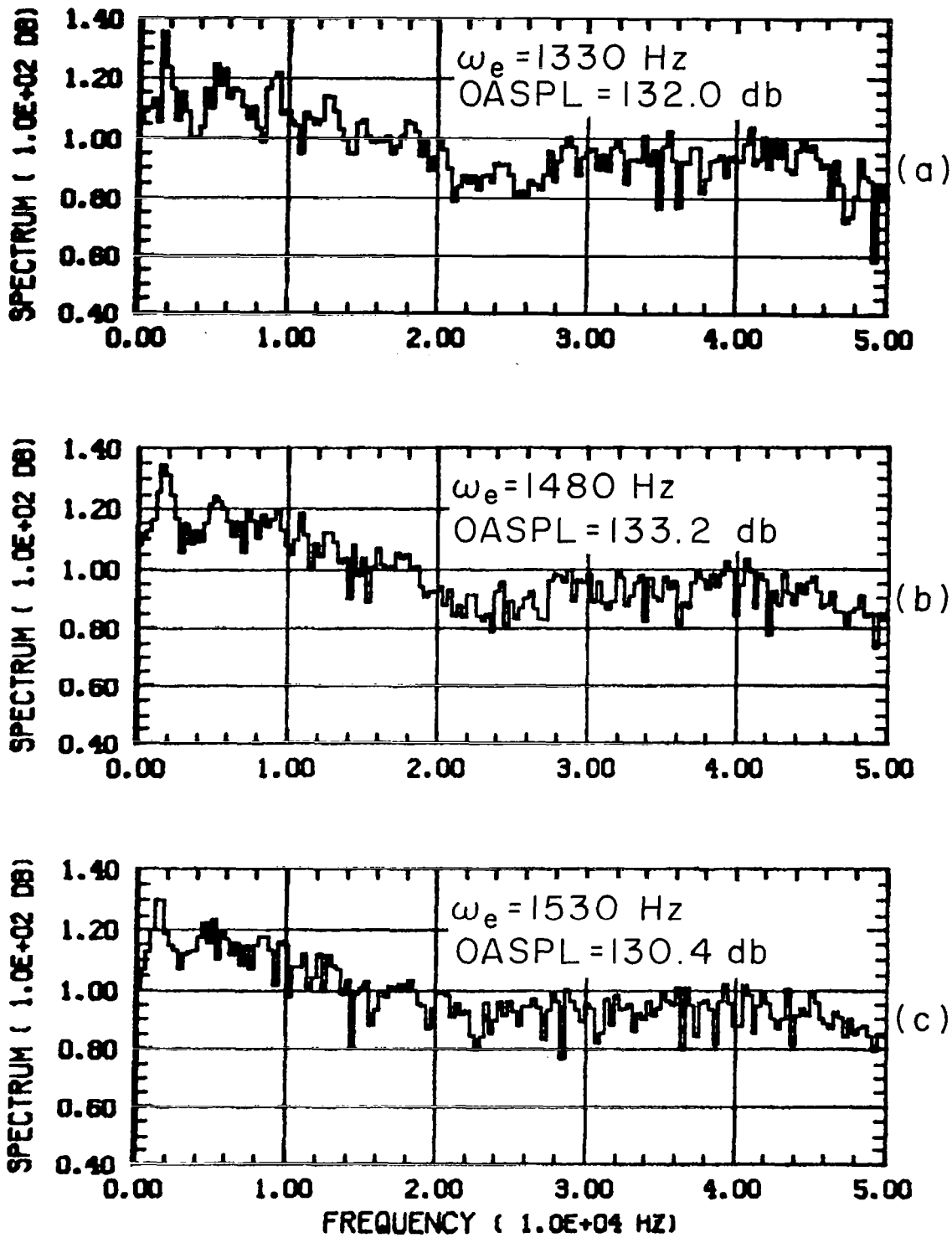

Figure 4.19 - Excited spectra of four vortices; phase = 135 degrees.

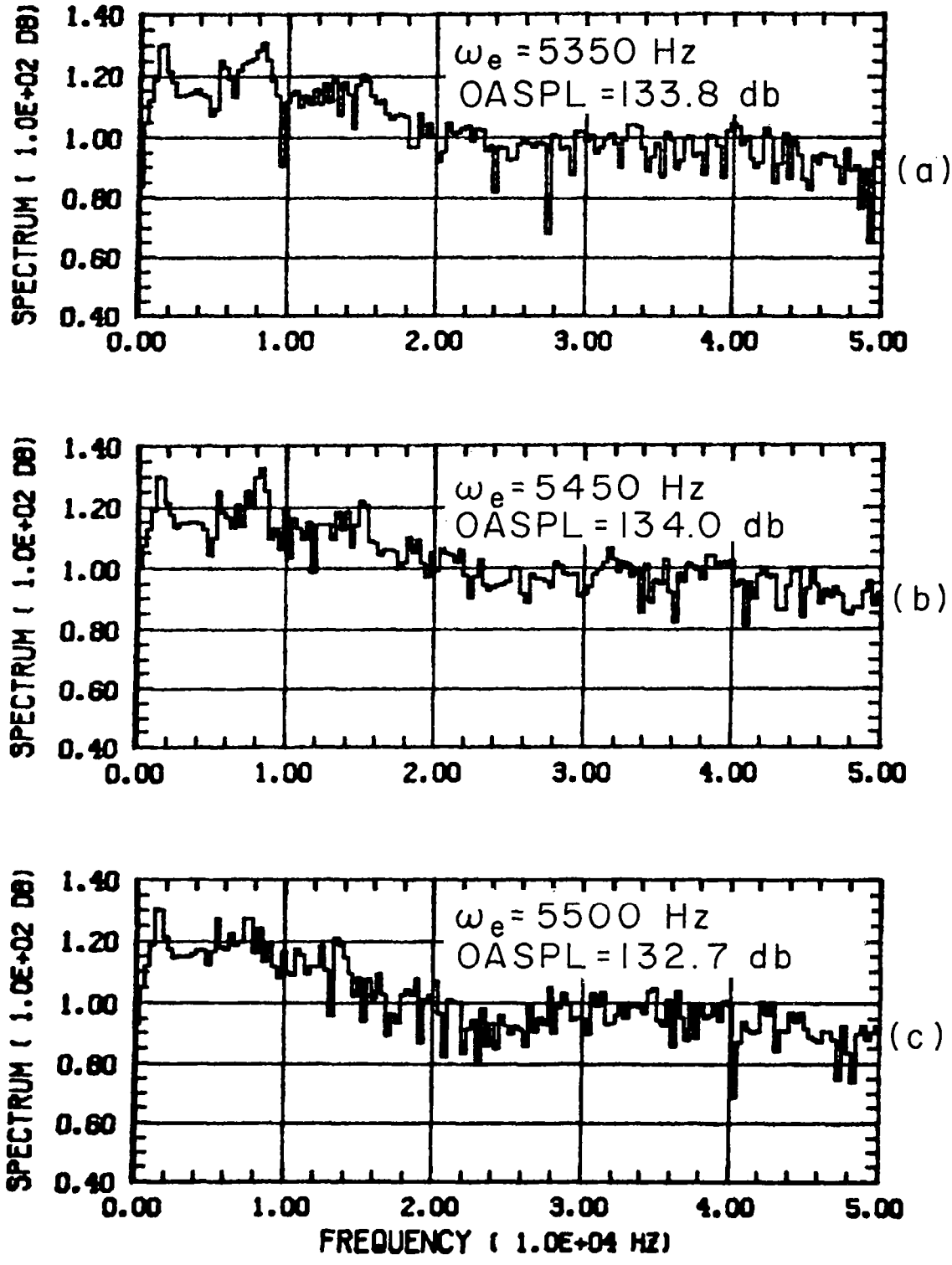

Figure 4.20 - Excited spectra of four vortices; phase = zero degree.

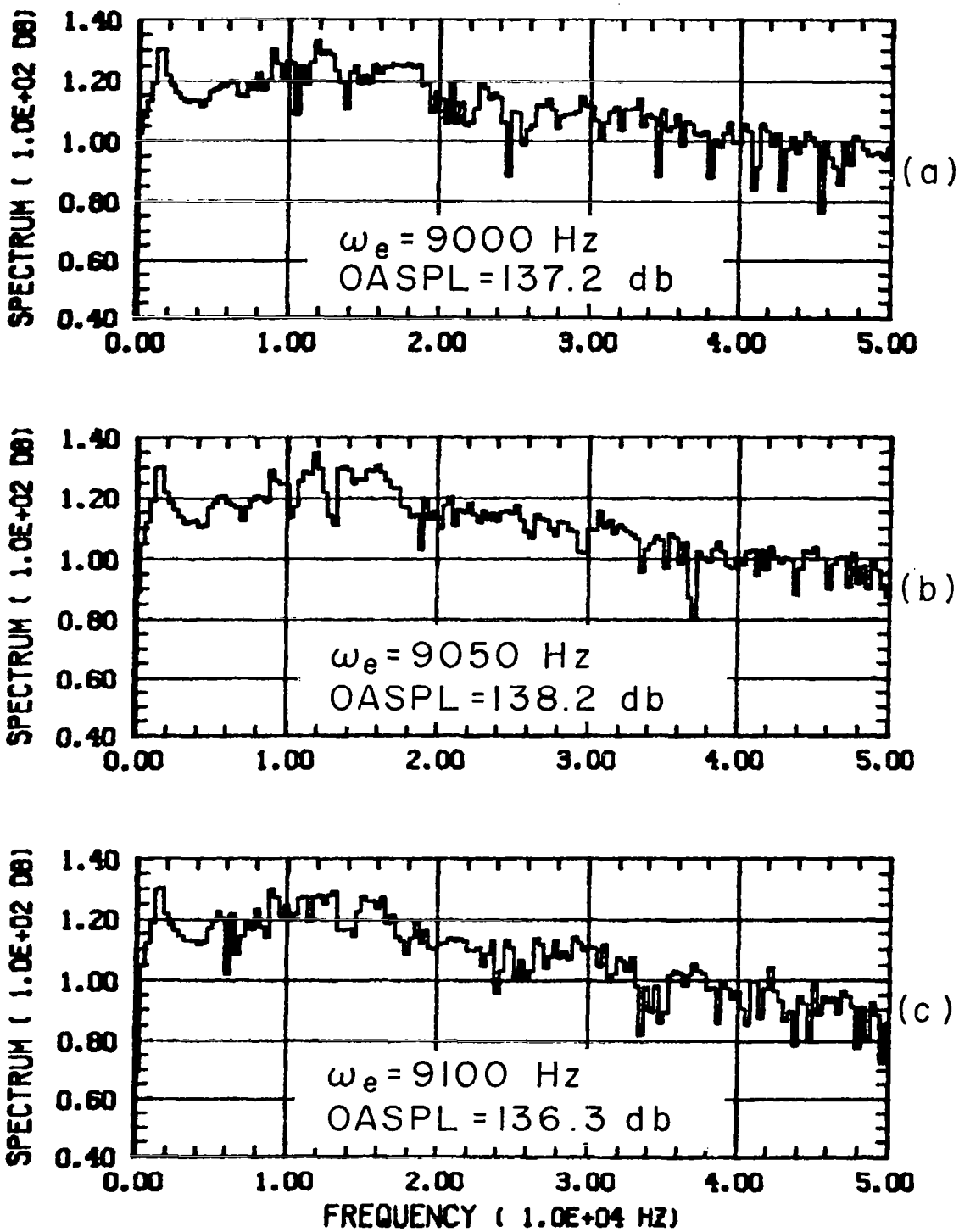

Figure 4.21 - High frequency excited spectra of four vortices; phase = zero degree (continued on next page).

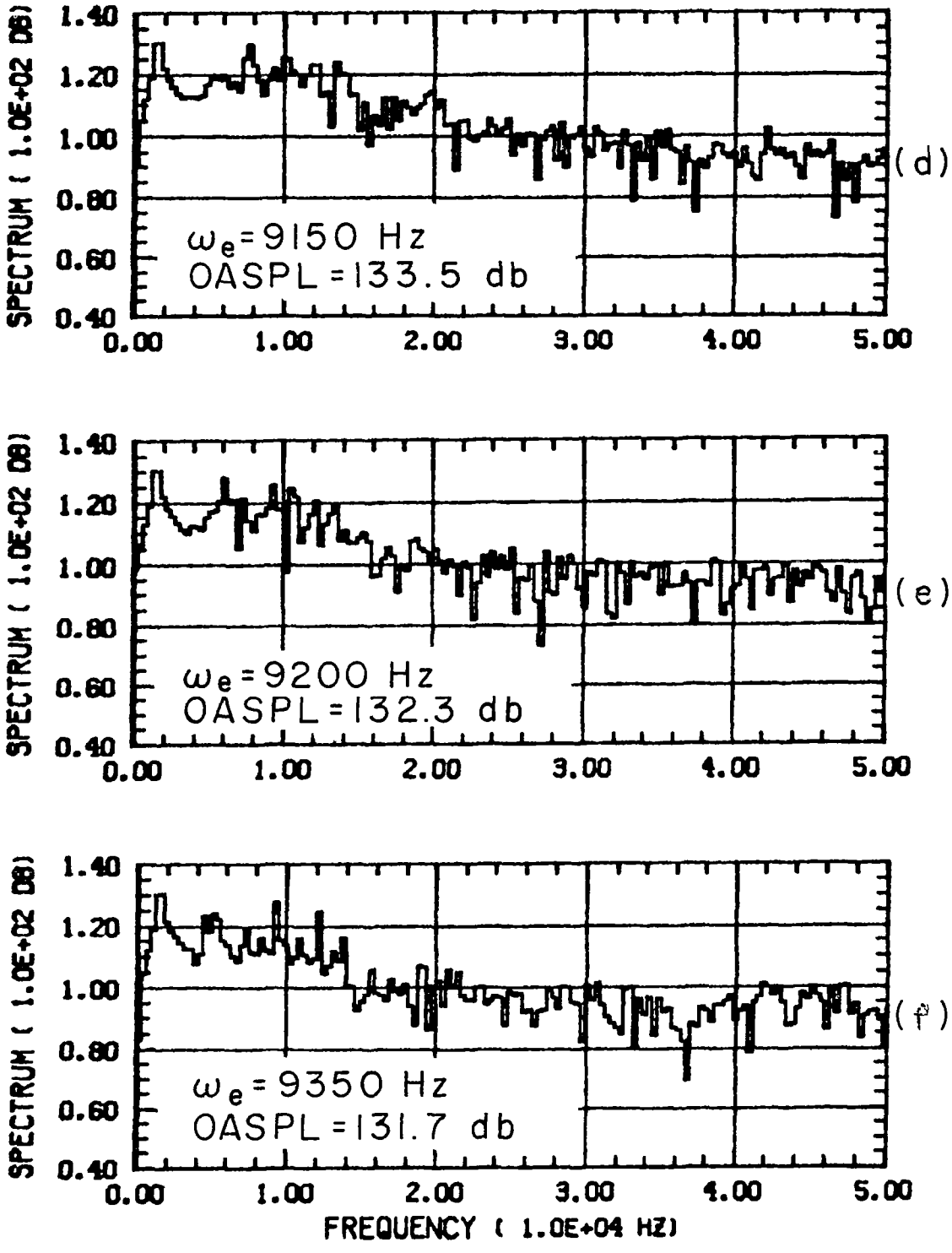

Figure 4.21 - High frequency excited spectra of four vortices; phase = zero degree (concluded).

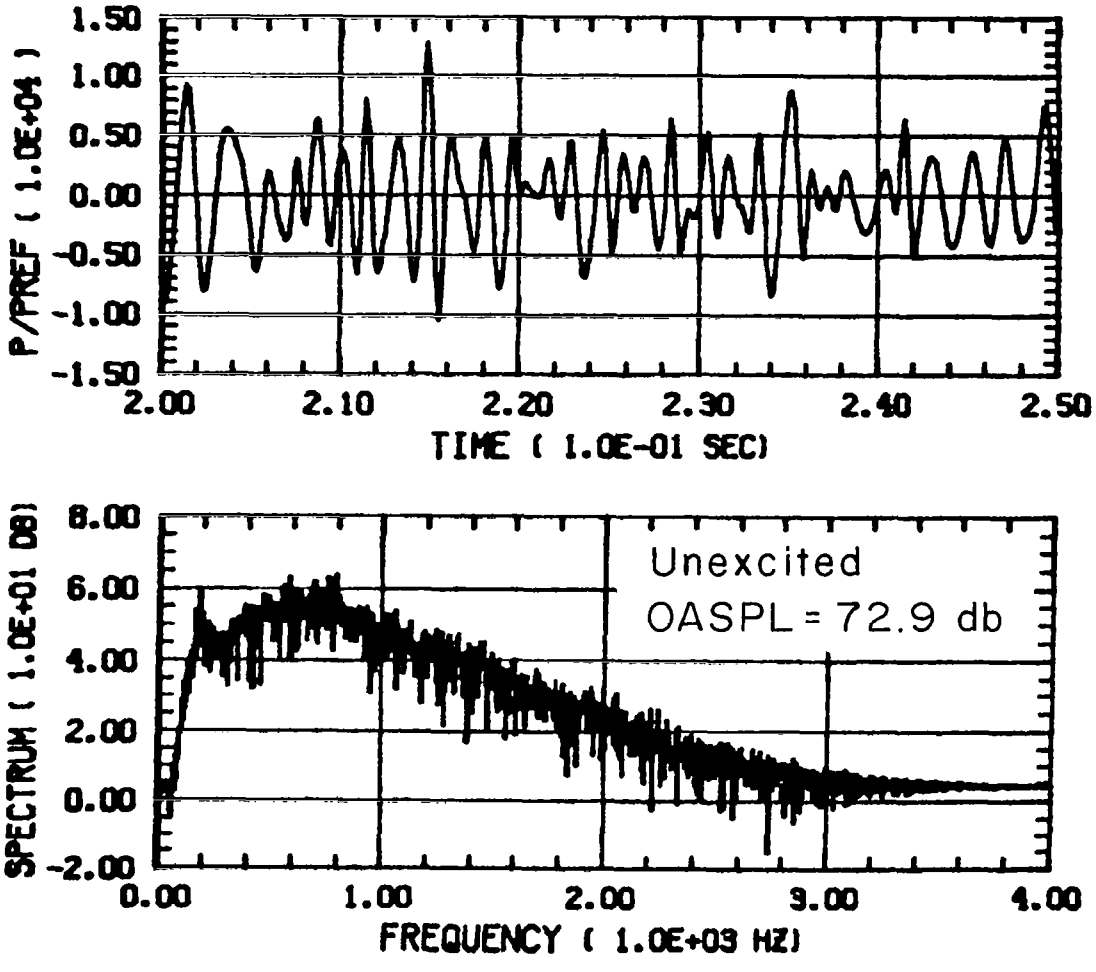

Figure 4.22 - Basic unexcited noise spectrum of six vortex array; γ_n = .2 m^2/sec.

TABLE 4.4 - ACOUSTIC EXCITATION OF SIX VORTICES

(EXCITATION ≅ 10% OF MAXIMUM VORTEX VELOCITY)

ω_e	OASPL (db)	Amplification (db)	Comments
0	72.9	0.0	Unexcited Array
100	73.1	0.2	
200	74.1	1.2	
300	74.4	1.5	
400	75.1	2.2	
412	75.5	2.6	Spectrum in Figure 4.23
425	74.6	1.7	
500	73.4	0.5	
600	73.2	0.3	
700	73.6	0.7	
750	76.7	3.8	Spectrum in Figure 4.24
775	76.8	3.9	
800	75.9	3.0	
900	73.5	0.6	
1000	79.2	6.3	Spectrum in Figure 4.25
1200	74.3	1.4	
1600	76.0	3.1	
2000	77.3	4.4	Spectrum in Figure 4.26

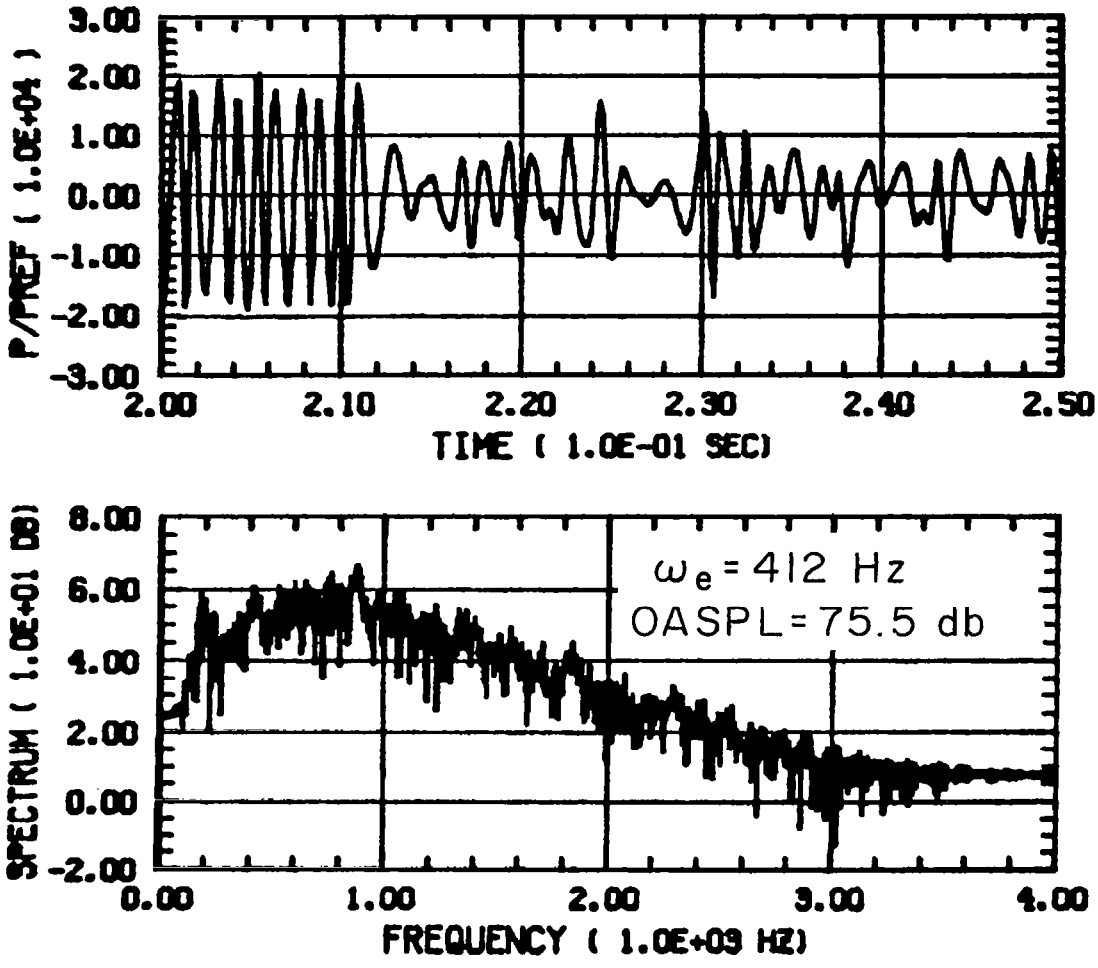

Figure 4.23 - Spectrum of excited six vortex array; ω_e = 412 Hz.

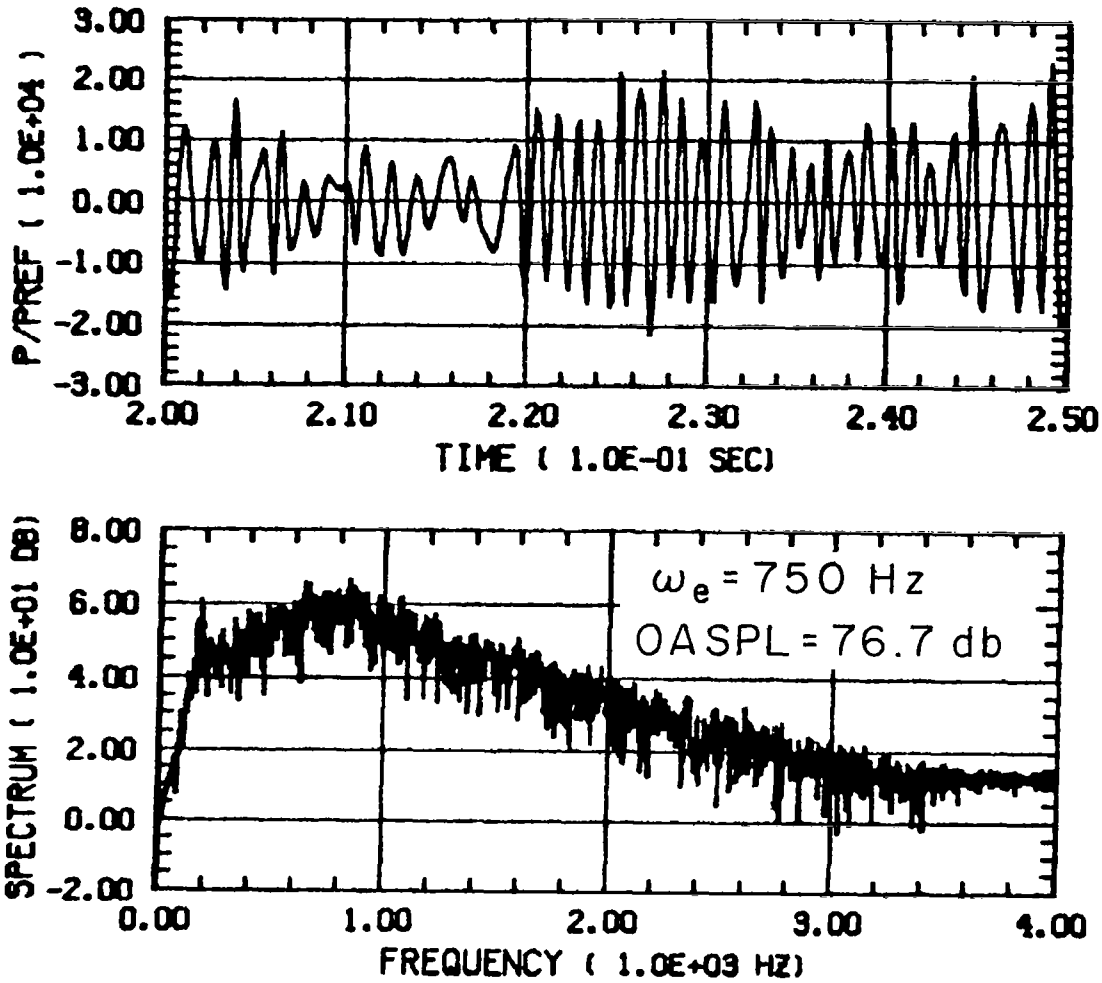

Figure 4.24 - Spectrum of excited six vortex array; ω_e = 750 Hz.

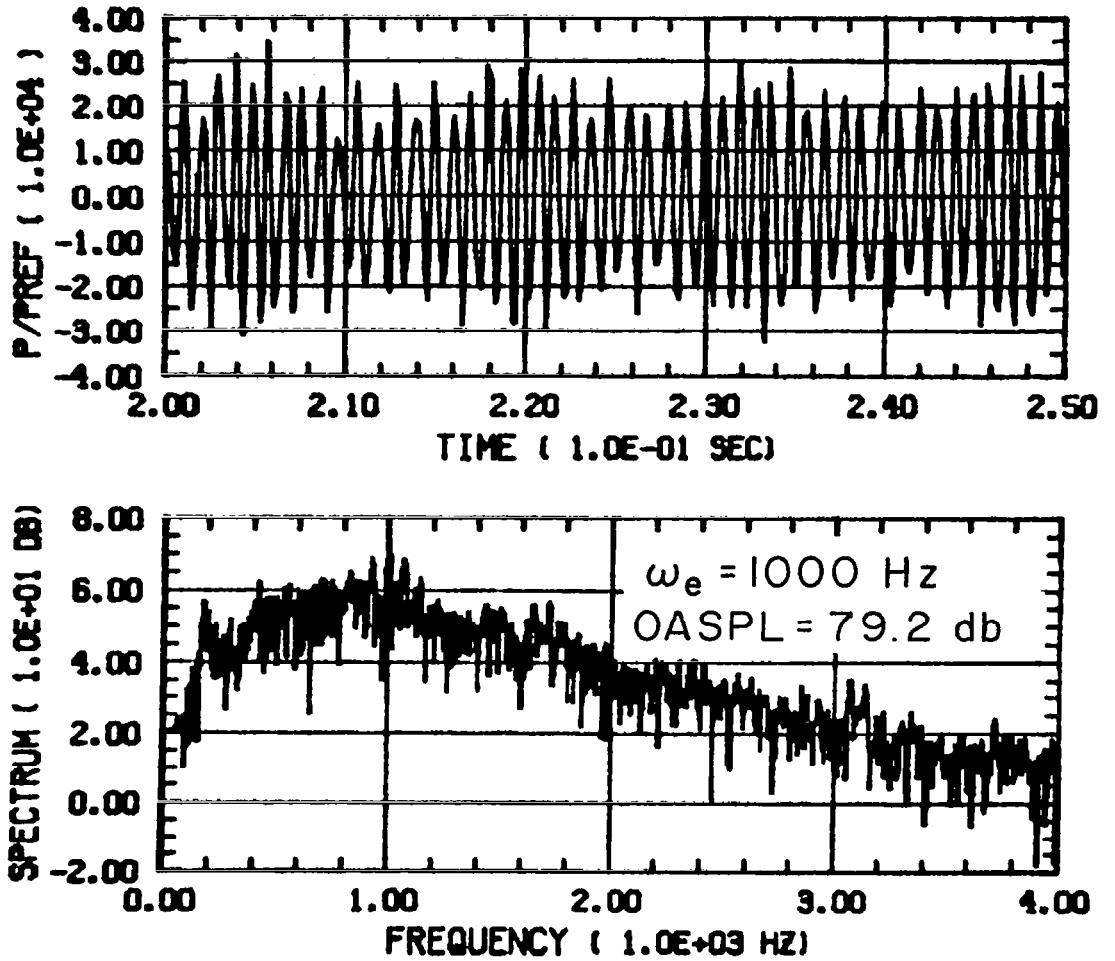

Figure 4.25 - Spectrum of excited six vortex array; ω_e = 1000 Hz.

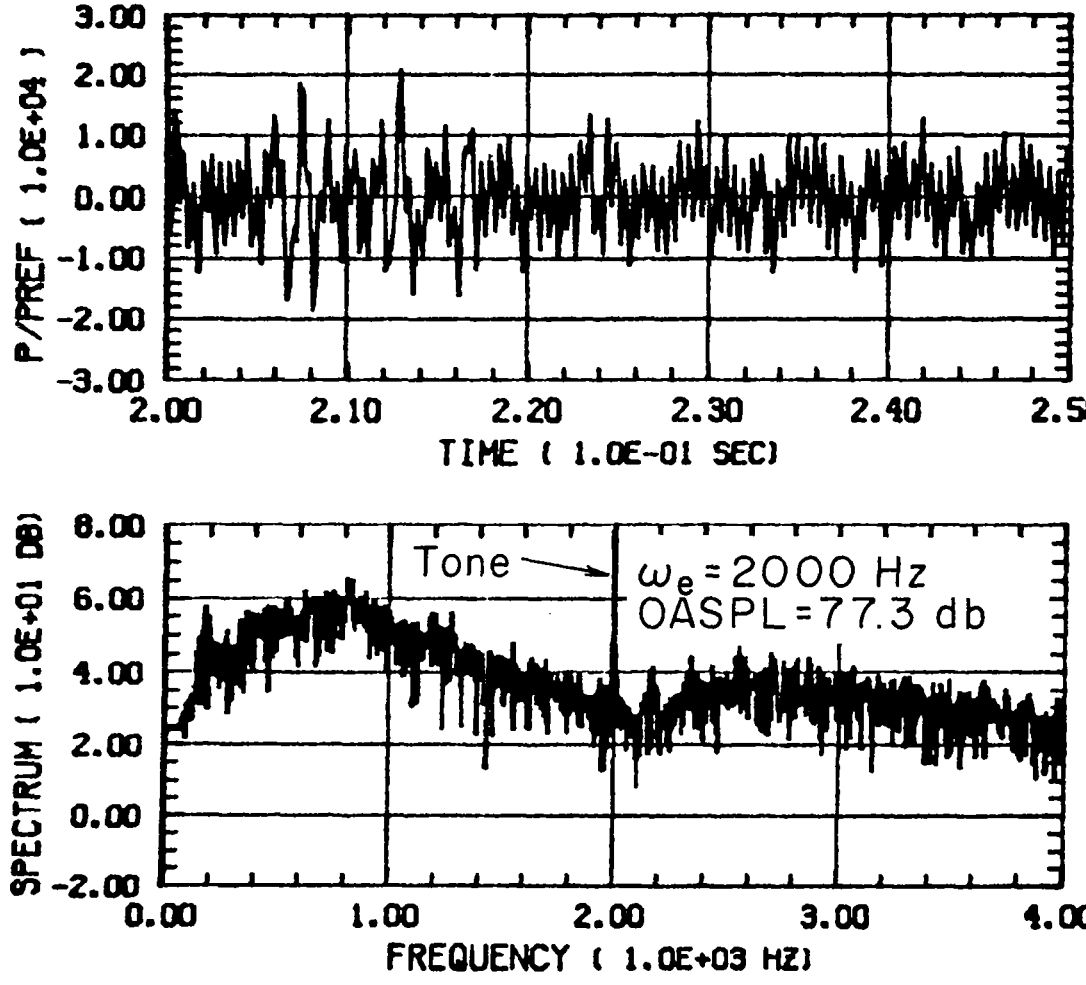

Figure 4.26 - Spectrum of excited six vortex array; ω_e = 2000 Hz.

V. CONCLUSION AND RECOMMENDATIONS

The general theory developed in Reference 1 has been further applied to the three basic problems of aeroacoustics; i.e.,

1) How is sound processed by a "primary" flow?

2) How is sound produced by a "primary" flow?

3) How does sound affect the primary flow?

The main conclusions are summarized below.

1) A general theory of sound scattering from low Mach number three-dimensional vortex flows is presented. The sound scattered from a vortex is proportional to the parameter $\Gamma k/a_\infty$ where Γ is the circulation, k the wave number, and a_∞ is the speed of sound.

2) An explicit formula and numerical calculation for plane wave scattering from a vortex ring is given. The forward scattering is much greater than the backscatter, but it is not singular as in the two-dimensional case.

3) The sound produced by a corotating vortex pair in various mean flows is calculated. A potential flow enhances the sound produced by the pair with little change in the fundamental frequency. Overtones in the spectrum are produced.

4) A shear flow rotating with the vortex pair increases the sound, shifts the basic frequency upward, and creates overtones in the spectrum. The radiation pattern is changed only slightly from isotropic.

5) A reverse shear flow reduces the pair noise, and for a sufficiently large shear the pair is annihilated. Reverse shear is a practical way of reducing the vortex pair noise mechanism.

6) A vortex pair near a wall (within one or two vortex spacings) radiates more noise than the corresponding free pair with its acoustic image in the wall. The radiation pattern becomes quadrupole in appearance with no noise radiated at 45 degrees to the wall.

7) Numerous calculations of vortex flow stimulation by externally applied sound are presented. A basic pair can be excited or attenuated by external sound near

resonance with the pair. The sound radiated by the pair is correspondingly enhanced or decreased. The mechanism of stimulated emission becomes more efficient as the Mach number of the pair is increased.

8) A collection of six vortices has a typical broadband noise spectrum. The array of vortices was ensonified with a pure tone over a wide band of frequencies. For frequencies near the knee of the spectrum the entire broadband noise spectrum was increased substantially. The amplification depends crucially on the nonlinear coupling between the vortices.

9) The calculations of stimulated emission of vortex noise are in quantitative agreement with experimental results (Refs. 2 and 3).

VI. REFERENCES

1. Yates, J.E.: Application of the Bernoulli Enthalpy Concept to the Study of Vortex Noise and Jet Impingement Noise. NASA CR-2987, 1978.

2. Bechert, D., and Pfizenmaier, E.: On the Amplification of Broadband Jet Noise by a Pure Tone Excitation. Proceedings of AIAA Aeroacoustics Conference, Palo Alto, CA, July 1976.

3. Parthasarathy, S.P., Cuffel, R., and Massier, P.F.: Influence of Internally Generated Pure Tones on the Broadband Noise Radiated from a Jet. AIAA, Vol. 16, No. 5, 1978, pp. 538-540.

4. Powell, A.: Theory of Vortex Sound. Aerodynamic Noise. September 1963, pp. 29-47.

5. Hardin, J.C.: Noise Calculation on the Basis of Vortex Flow Models. Presented at ASME Symposium on Noise and Fluids Engineering, Atlanta, GA, November 28-30, 1977.

6. Adams, J.C., et. al., eds.: NCAR Software Support Library-Volume 2. NCAR-TN/1A-105, National Center for Atmospheric Research, March 1975.

7. Hardin, J.C.: Analysis of Noise Produced by an Orderly Structure of Turbulent Jets. NASA TN-7242, 1973.

8. Davies, P.O.A.L., Hardin, J.C., Edwards, A.V.J., and Mason, J.P.: A Potential Flow Model for Calculation of Jet Noise. Aeroacoustics: Jet Noise, Combustion and Core Engine Noise, edited by I.R. Schwartz, AIAA, Vol. 43, March 1975.